Efficient Solution of Two-Dimensional Wave Propagation Problems by CQ-Wavelet BEM: Algorithm and Applications

SIAM J. SCI. COMPUT.
Vol. 42, No. 4, pp. B894–B920

EFFICIENT SOLUTION OF TWO-DIMENSIONAL WAVE PROPAGATION PROBLEMS BY CQ-WAVELET BEM: ALGORITHM AND APPLICATIONS*

LUCA DESIDERIO† AND SILVIA FALLETTA‡

Abstract. In this paper we consider wave propagation problems in two-dimensional unbounded domains, including dissipative effects, reformulated in terms of space-time boundary integral equations. For their solution, we employ a convolution quadrature (CQ) for the temporal and a Galerkin boundary element method (BEM) for the spatial discretization. It is known that one of the main advantages of the CQ-BEMs is the use of the FFT algorithm to retrieve the discrete time integral operators with an optimal linear complexity in time, up to a logarithmic term. It is also known that a key ingredient for the success of such methods is the efficient and accurate evaluation of all the integrals that define the matrix entries associated to the full space-time discretization. This topic has been successfully addressed when standard Lagrangian basis functions are considered for the space discretization. However, it results that, for such a choice of the basis, the BEM matrices are in general fully populated, a drawback that prevents the application of CQ-BEMs to large-scale problems. In this paper, as a possible remedy to reduce the global complexity of the method, we consider approximant functions of wavelet type. In particular, we propose a numerical procedure that, by taking advantage of the fast wavelet transform, allows us on the one hand to compute the matrix entries associated to the choice of wavelet basis functions by maintaining the accuracy of those associated to the Lagrangian basis ones and, on the other hand, to generate sparse matrices without the need of storing a priori the fully populated ones. Such an approach allows in principle the use of wavelet basis of any type and order, combined with CQ based on any stable ordinary differential equations solver. Several numerical results, showing the accuracy of the solution and the gain in terms of computer memory saving, are presented and discussed.

Key words. damped wave equation, convolution quadrature, boundary element method, wavelets

AMS subject classification. 65M38

DOI. 10.1137/19M1287614

1. Introduction.

Computational methods for solving time-domain formulations of wave equation problems have been an active area of research, developed in conjunction with fields such as acoustics, seismology, geophysics, and meteorology. The model of interest may be a pure or a damped wave equation. The latter provides a much better description of the phenomenon, since it takes into account the ability of the possible energy dissipation produced by the system.

A very difficult point is that many problems are set in unbounded domains, making the design of suitable and accurate numerical methods very challenging. The boundary integral equation (BIE) technique, whose discretization is known as the boundary element method (BEM), has emerged as an efficient alternative to all the classical domain methods, because it allows one to handle problems defined on the

*Submitted to the journal's Computational Methods in Science and Engineering section December 9, 2019; accepted for publication (in revised form) April 24, 2020; published electronically July 6, 2020.

https://doi.org/10.1137/19M1287614

Funding: This work was partially supported by MIUR grant Dipartimenti di Eccellenza 2018-2022, by the GNCS-INDAM 2018 research program "Sviluppo di tecniche efficienti e accurate per metodi BEM," and by the GNCS-INDAM 2019 research program "Metodi di approssimazione locale con applicazioni all'analisi isogeometrica e alle equazioni integrali di contorno."

†Department of Mathematical, Physical and Computer Science, University of Parma, 43124 Parma, Italy (Luca.desiderio@unipr.it).

‡Department of Mathematical Sciences "G.L. Lagrange," Politecnico di Torino, 10129 Torino, Italy (silvia.falletta@polito.it).

exterior of bounded domains as easily as those defined in the interior of bounded domains.

For space-time domain wave propagation problems without damping, the application of BIE techniques began to be analyzed in the 1980s with the pioneering work by Bamberger and Ha Doung [6]. In recent years, several other approaches have been proposed for solving standard wave equation problems by means of BIEs, directly in the space-time domain. Among these we mention here the Lubich convolution quadrature (CQ) [41] and the energetic technique [2]. These have been recently extended to two-dimensional (2D) damped wave propagation problems in [13] and [4, 5], respectively. However, the development of efficient and reliable BIE strategies to simulate time-domain waves in unbounded exterior domains is still a numerical challenge and a subject of active recent research, the main aim being the reduction of the computational complexity and of the high memory required to compute and store all the entries of the matrices associated to the discrete boundary integral operators. Indeed, it is known that, when standard Lagrangian basis functions are considered for the space approximation, the BEM matrices are generally fully populated, and the overall memory cost of the BEM is $O(M^2N)$, M and N being the number of grid points chosen on the domain boundary and the total number of time steps performed, respectively. This drawback prevents the application of such methods to large-scale realistic problems.

In recent years the development of fast numerical methods for the efficient and reliable simulation of scattered waves in unbounded exterior domains has improved the application of BEMs. For problems in three spatial dimensional domains, fast versions of the CQ with backward differentiation formulas (BDF) of order 2 for the temporal discretization have been developed in [7, 28, 32, 38] and with Runge–Kutta convolution weights in [11, 12]. Among other effective techniques, aiming at reducing computational cost and memory storage, we mention the fast multiple method [29], panel clustering [26, 30], and hierarchical matrices [31]. For recent developments of the fast multiple method in the context of wave propagation see [45], while for recent developments in hierarchical matrices we also refer to [16, 19]. It is also worth mentioning the recent papers [1] and [40], in which interesting time-domain FEM-BEM and wavelet BEM methods, respectively, applied to large-scale industrial problems are shown.

In this paper, we consider 2D exterior wave propagation problems, including a dissipative term. We apply a numerical scheme which is based on the discrete CQ formulas, proposed by Lubich [41], for the discretization in time. The CQ formulas have the fundamental property of using the Laplace transform of the kernel of the integral equation instead of its space-time expression, the former having better regularity properties. Due to the possibility of reducing the computational complexity of the time discretization to order $N \log N$, thanks to the use of a fast fourier transform (FFT), this approach has become a very appealing tool for the numerical simulation of wave propagation problems. A thorough review of results and properties of CQ applied to BIEs can be found in [9]. In recent years, CQ formulas associated with A-stable BDF of order $k \leq 2$ [43] have been successfully applied to wave propagation problems in two and three dimensions with the Dirichlet boundary condition [21] and in two dimensions with Neumann and mixed boundary conditions [22, 44]. The Lubich technique has been also efficiently used for the time approximation of nonreflecting boundary conditions for solving exterior problems by the finite element method (FEM) [23, 24, 27].

In combination with the CQ, for the discretization in space, we consider a Galerkin method based on wavelet approximating functions. It is known that the wavelets have

the property of yielding sparse matrices when applied to a wide class of pseudodifferential operators [15]. Wavelet BEMs have been widely applied, for example in [33, 37, 39], to solve stationary problems. Very recently, in [14], Bertoluzza, Falletta, and Scuderi have applied a CQ-wavelet method to the wave equation with Dirichlet boundary conditions. In particular, they have proposed a wavelet compression technique, combined with a time downsampling FFT strategy, that allows one to obtain highly sparse BEM matrices with a computational complexity of order $\widetilde{N} \log \widetilde{N}$, where $\widetilde{N} \ll N$. Based on the expansion of the unknown solution in terms of the reconstruction wavelet functions of the BIOR2.2 wavelet basis, and on an a priori estimate of the decaying behavior in time of the matrix entries, this strategy allows us to compute only those elements which are significant with respect to a prescribed tolerance. The main drawback of this approach is that it can be applied if the explicit expression of the wavelet basis functions is known and that it requires ad hoc quadrature strategies to compute the matrix entries, defined by space integrals, with sufficiently high accuracy. Having also long-time computation in mind, we recall that the accurate calculation of such matrix entries represents a key issue for the success of any CQ-BEM. Indeed, the more accurate their evaluation, the larger the time interval where the method is faithful. This topic has been successfully addressed when standard Lagrangian basis functions are considered for the space discretization [21, 22, 25], while it is not well established yet in the CQ-wavelet BEM case. In particular, an accurate quadrature rule may become demanding if high order wavelet bases are considered or even impossible if, for example, wavelets are not given in analytic form.

We are aware that in the context of wavelet BEM much effort has been made to design efficient algorithms and quadrature rules for time independent problems [20, 33, 34, 35, 36]. These papers show how the BEM matrices can be approximated by sparse ones for fixed time instants. However, this strategy would imply the loss of the FFT routine, and hence of the CQ-BEM efficiency, in the construction step of the matrices, the latter being a feature which instead we aim at preserving.

The goal of this work is to propose a purely algorithmic procedure to obtain sparse BEM matrices by combining the CQ-BEM with a Galerkin wavelet method. The approach is based on the accurate computation of the matrix entries, defined by space integrals, in terms of piecewise linear Lagrangian basis functions. By maintaining the same accuracy, the matrix entries in terms of the wavelet basis are then retrieved by taking advantage of the fast discrete wavelet transform (DWT). We will show that the new strategy allows the use of wavelet basis of any type and order, even not known in closed form. We remark that the latter are of particular interest when the wavelet approximation is combined with CQ based on A-stable ordinary differential equation (ODE) solvers that give rise to highly oscillating convolution weights. This is the case, for example, when the trapezoidal CQ-rule is applied to the pure wave equation, or to the dissipative one when the dissipation strongly dominates on the speed of propagation. In these cases, the use of low order wavelet basis, such as the BIOR2.2, does not produce matrices that are as sparse as those obtained, for example, in [14]. We will show indeed that if the number of the wavelet vanishing moments, which plays a key role in the sparsification, is not high enough, the decay to zero (with respect to time) of the BEM wavelet matrix entries can be severely affected. The use of wavelets with a bigger number of vanishing moments will allow us to retrieve higher sparse matrices.

Moreover, we will apply a compression strategy that, as we will show, allows us to get sparse matrices without the need for storing a priori all the fully populated ones associated to the use of the piecewise linear Lagrangian basis functions.

We present an extensive numerical investigation of the sparsification properties of the wavelet approach with respect to the variation of the damped equation parameters, to the choice of the wavelet basis and of the CQ method. Incidentally, we remark that the analysis of the sparsity of the matrices associated to the single and double layer operators is also of interest when the BEM wavelet is used to define a transparent boundary condition in a FEM-BEM (or finite differences-BEM) coupling.

The paper is organized as follows. In the next section we introduce the damped wave equation, with Dirichlet and Neumann type boundary conditions, and its reformulation in terms of space-time BIEs. In section 3 we describe the main steps that lead to the time CQ formulas associated to BIEs of the first and second kind and the principles of the standard Galerkin BEM. In section 4 we introduce the wavelet framework and the DWT and we describe the algorithmic procedure for the compression of the CQ-BEM matrices. Then, in section 5 we present numerical results concerning the study of the sparsity behavior of the matrices associated to the BEM operators with respect to the variation of the damped wave equation parameters; furthermore, several numerical tests show the effectiveness of the sparsification, in terms of memory saving and accuracy. Some conclusions are then drawn in section 6.

2. The model problem. Let $\Omega \subset \mathbf{R}^2$ denote an open, bounded domain with a sufficiently smooth closed boundary $\Gamma := \partial\Omega$ and let $\Omega^e := \mathbf{R}^2 \setminus \overline{\Omega}$. We consider the following exterior problems given by the scalar damped wave equation in absence of body forces and with a Dirichlet boundary condition,

$$\begin{cases} \Delta u(\mathbf{x};t) - \alpha \dot{u}(\mathbf{x};t) - \frac{1}{c^2}\ddot{u}(\mathbf{x};t) = 0, & (\mathbf{x};t) \in \Omega^e \times (0,T), \\ u(\mathbf{x};0) = \dot{u}(\mathbf{x};0) = 0, & \mathbf{x} \in \Omega^e, \\ u(\mathbf{x};t) = f(\mathbf{x};t), & (\mathbf{x};t) \in \Gamma \times (0,T), \end{cases} \tag{2.1}$$

or with a Neumann boundary condition,

$$\begin{cases} \Delta u(\mathbf{x};t) - \alpha \dot{u}(\mathbf{x};t) - \frac{1}{c^2}\ddot{u}(\mathbf{x};t) = 0, & (\mathbf{x};t) \in \Omega^e \times (0,T), \\ u(\mathbf{x};0) = \dot{u}(\mathbf{x};0) = 0, & \mathbf{x} \in \Omega^e, \\ \frac{\partial u}{\partial \mathbf{n}}(\mathbf{x};t) = g(\mathbf{x};t), & (\mathbf{x};t) \in \Gamma \times (0,T). \end{cases} \tag{2.2}$$

In problems (2.1) and (2.2), $u(\mathbf{x};t)$ is the unknown displacement field, $\alpha \geq 0$ is the *damping parameter*, and $c > 0$ is the *wave propagation speed* in the medium. These last two parameters are related by $\alpha \cdot c^2 := 1/\bar{\tau}$, with $\bar{\tau} \geq 0$ known as *relaxation time*. Furthermore, the superposed dot indicates time differentiation, while Δ denotes the Laplace operator. In the boundary conditions, the prescribed values are indicated by f and g and, with reference to the domain Ω^e, $\mathbf{n}$ denotes the unit outward normal vector to the boundary Γ.

Let $G(r;t)$ denote the forward fundamental solution of the 2D damped wave equation [4]:

$$G(r;t) := \frac{c}{2\pi} \cosh\left(\frac{\alpha}{2} c\sqrt{c^2t^2 - r^2}\right) \frac{H(ct-r)}{\sqrt{c^2t^2 - r^2}} e^{-\frac{\alpha}{2}c^2 t} \tag{2.3}$$

with $r := \|\mathbf{x} - \mathbf{y}\|$ and $H(\cdot)$ the Heaviside distribution. Note that, when $\alpha = 0$, we have the fundamental solution of the 2D wave equation.

We consider the boundary element reformulation of (2.1) and (2.2) in terms of the following single layer space-time integral potential:

$$u(\mathbf{x};t) = \int_\Gamma \int_0^t G(\|\mathbf{x} - \mathbf{y}\|; t-\tau)\varphi(\mathbf{y};\tau) d\Gamma_{\mathbf{y}} d\tau, \qquad (\mathbf{x};t) \in \Omega^e \times (0,T), \tag{2.4}$$

where $\varphi(\mathbf{x};t)$ is a continuous density function, representing the jump of the normal derivative of the solution of problem (2.1) or (2.2) along the boundary. The single layer potential $u(\mathbf{x};t)$ is a solution of the Dirichlet problem (2.1) provided $\varphi(\mathbf{x};t)$ is the solution of the time dependent BIE (TD-BIE) of the first kind,

$$\int_\Gamma \int_0^t G(\|\mathbf{x}-\mathbf{y}\|;t-\tau)\varphi(\mathbf{y};\tau)d\Gamma_{\mathbf{y}}d\tau = f(\mathbf{x};t), \qquad (\mathbf{x};t)\in\Gamma\times(0,T), \tag{2.5}$$

while it is a solution of the Neumann problem (2.2) provided $\varphi(\mathbf{x};t)$ is the solution of the TD-BIE of the second kind,

$$\frac{1}{2}\varphi(\mathbf{x};t) - \int_\Gamma \int_0^t \frac{\partial G}{\partial \mathbf{n}_{\mathbf{x}}}(\|\mathbf{x}-\mathbf{y}\|;t-\tau)\varphi(\mathbf{y};\tau)d\Gamma_{\mathbf{y}}d\tau = g(\mathbf{x};t), \qquad (\mathbf{x};t)\in\Gamma\times(0,T), \tag{2.6}$$

where $\mathbf{n}_{\mathbf{x}}$ is the outward boundary unit normal vector at $\mathbf{x}\in\Gamma$.

Remark 2.1. For possible volume terms in (2.5) and (2.6) generated by nontrivial sources and nonhomogeneous initial conditions, we refer to [21, 22]. These will contribute to the right-hand side (RHS) of the final linear system, hence they will not influence the analysis of the method we are going to present in the next sections.

3. Galerkin Lubich CQ-BEM. To approximate the solution of (2.5) and (2.6), we present a numerical approach that combines a Lubich CQ-method based on A-stable ODE methods with a classical wavelet Galerkin method [41]. In the following section we provide a very brief description of the CQ approach for the time discretization. The reader is referred to [43] for further details.

3.1. Time discretization. For the time discretization, we split the interval $[0,T]$ into N steps of equal length $\Delta t = T/N$. Collocating (2.5) and (2.6) at the discrete time instant $t_n := n\Delta t$, we obtain

$$\int_\Gamma \int_0^{t_n} G(\|\mathbf{x}-\mathbf{y}\|;t_n-\tau)\varphi(\mathbf{y};\tau)d\Gamma_{\mathbf{y}}d\tau = f(\mathbf{x};t_n), \qquad \mathbf{x}\in\Gamma,\ \ n=0,\dots,N, \tag{3.1}$$

and

$$\frac{1}{2}\varphi(\mathbf{x};t_n) - \int_\Gamma \int_0^{t_n} \frac{\partial G}{\partial \mathbf{n}_{\mathbf{x}}}(\|\mathbf{x}-\mathbf{y}\|;t_n-\tau)\varphi(\mathbf{y};\tau)d\Gamma_{\mathbf{y}}d\tau = g(\mathbf{x};t_n), \qquad \mathbf{x}\in\Gamma,\ \ n=0,\dots,N. \tag{3.2}$$

The semidiscrete approximations φ_n of the unknown density $\varphi(\cdot;t_n)$ are obtained by solving

$$\sum_{j=0}^{n}\int_\Gamma \omega^{\mathcal{V}}_{n-j}(\|\mathbf{x}-\mathbf{y}\|;\Delta t)\varphi_j(\mathbf{y})d\Gamma_{\mathbf{y}} = f_n(\mathbf{x}), \qquad \mathbf{x}\in\Gamma,\ n=0,\dots,N, \tag{3.3}$$

or

$$\frac{1}{2}\varphi_n(\mathbf{x}) - \sum_{j=0}^{n}\int_\Gamma \omega^{\mathcal{K}}_{n-j}(\|\mathbf{x}-\mathbf{y}\|;\Delta t)\varphi_j(\mathbf{y})d\Gamma_{\mathbf{y}} = g_n(\mathbf{x}), \qquad \mathbf{x}\in\Gamma,\ n=0,\dots,N. \tag{3.4}$$

To simplify the notation, in (3.3) and (3.4) we have set $f_n(\mathbf{x}) := f(\mathbf{x};t_n)$ and $g_n(\mathbf{x}) := g(\mathbf{x};t_n)$. In the following, we will refer to $\omega^{\mathcal{J}}_n(r;\Delta t)$, with $\mathcal{J}=\mathcal{V},\mathcal{K}$, as convolution weights associated to the kernels of the corresponding integral operators.

The weights are computed by using the contour integral representation

$$\omega_n^{\mathcal{J}}(r;\Delta t) = \frac{1}{\imath 2\pi}\oint_{|z|=\varrho} \widehat{G}^{\mathcal{J}}\left(r;\frac{\gamma(z)}{\Delta t}\right) z^{-(n+1)}dz, \tag{3.5}$$

where $\widehat{G}^{\mathcal{V}}(r;s) = \widehat{G}(r;s)$ is the Laplace transform of kernel G appearing in (2.5), and $\widehat{G}^{\mathcal{K}}(r;s) = \widehat{\frac{\partial G}{\partial \mathbf{n}}}(r;s)$ is the Laplace transform of the kernel $\frac{\partial G}{\partial \mathbf{n}}$ appearing in (2.6), i.e.,

$$\widehat{G}^{\mathcal{V}}(r;s) := \frac{1}{2\pi}K_0\left(\frac{r}{c}\sqrt{s^2+\alpha s}\right) \text{ and } \widehat{G}^{\mathcal{K}}(r;s) := -\frac{\sqrt{s^2+\alpha s}}{2\pi c}\ \frac{\mathbf{r}\cdot\mathbf{n}_{\mathbf{x}}}{r}K_1\left(\frac{r}{c}\sqrt{s^2+\alpha s}\right), \tag{3.6}$$

having denoted by K_0 and K_1 the modified Bessel functions of second kind and of order 0 and 1, respectively. In (3.5), $\gamma(z)$ denotes the characteristic quotient of an ODE solver, and the parameter ϱ is such that the circle $|z| \le \varrho$ lies in the domain of analyticity of $\widehat{G}^{\mathcal{J}}\left(r;{}^{\gamma(z)}/_{\Delta t}\right)$. Among the most commonly used A-stable ODE solvers, we recall the expression of $\gamma(z)$ associated to the BDF of order 2 (BDF2) and to the trapezoidal rule (TRAP)

$$\gamma(z) = \begin{cases} \frac{z^2}{2} - 2z + \frac{3}{2} & \text{BDF2,} \\ 2\frac{1-z}{1+z} & \text{TRAP,} \end{cases}$$

which we are going to consider as a benchmark in the forthcoming sections. In principle, any A-stable ODE solver can be applied. We recall that convergence results for the trapezoidal rule, that were not provided in [41], have been later derived in [8].

It is known that for certain time stepping schemes it is possible to determine the $\omega_n^{\mathcal{J}}$ explicitly [10, 26, 38]. In such cases, efficient methods such as panel clustering or the fast and oblivious CQ algorithm have been proposed.

In general, however, for a fixed value of r, the convolution weights are efficiently approximated, by introducing the polar coordinate $z = \varrho e^{\imath\theta}$ and by using the trapezoidal rule with $\tilde{R}$ equal steps of length ${}^{2\pi}/_{\tilde{R}}$, i.e.,

$$\omega_n^{\mathcal{J}}(r;\Delta t) \simeq \frac{\varrho^{-n}}{\tilde{R}}\sum_{l=0}^{\tilde{R}-1} \widehat{G}^{\mathcal{J}}\left(r;\frac{\gamma\left(\varrho e^{\imath l\frac{2\pi}{\tilde{R}}}\right)}{\Delta t}\right) e^{-\imath n l\frac{2\pi}{\tilde{R}}}. \tag{3.7}$$

All the $\omega_n^{\mathcal{J}}(r;\Delta t)$ are then computed simultaneously by the FFT algorithm with $\mathcal{O}(\tilde{R}\log\tilde{R})$ flops.

Remark 3.1. In the design of efficient tools for the CQ-BEM, the behavior of $\omega_n^{\mathcal{J}}(r;\Delta t)$ plays a key role; see again [10, 26, 38]. Moreover, such a behavior depends both on the parameters c and α and on the function $\gamma(z)$.

As an example, in Figures 1 and 2 we show the graph of $\omega_n^{\mathcal{V}}(r;\Delta t)$ (that of $\omega_n^{\mathcal{K}}(r;\Delta t)$ is similar) associated to the pure wave equation ($c = 1\cdot{}^{\mathrm{m}}/_{\mathrm{s}}$, $\alpha = 0\cdot{}^{\mathrm{m}^2}/_{\mathrm{s}}$) and to the dissipative one, respectively. In the second case, the values of $c = 9685\cdot{}^{\mathrm{m}}/_{\mathrm{s}}$ and $\alpha = 1.1\times 10^4\cdot{}^{\mathrm{m}^2}/_{\mathrm{s}}$ refer to the material parameters of silicon [42].

As we can see, for the wave equation without damping, when the BDF2 method is considered (Figure 1, top row), the $\omega_n^{\mathcal{V}}(r;\Delta t)$ are defined for $r > 0$, have a peak around $r \approx t_n$, decay exponentially for $r \gg t_n$, and have a "tail" toward $r = 0$ which is not tending to zero. On the other hand, when the TRAP method is considered, the very smooth behavior of the coefficients along the tail is replaced by a highly oscillating one (see Figure 1, bottom row). In the dissipative case (Figure 2), because

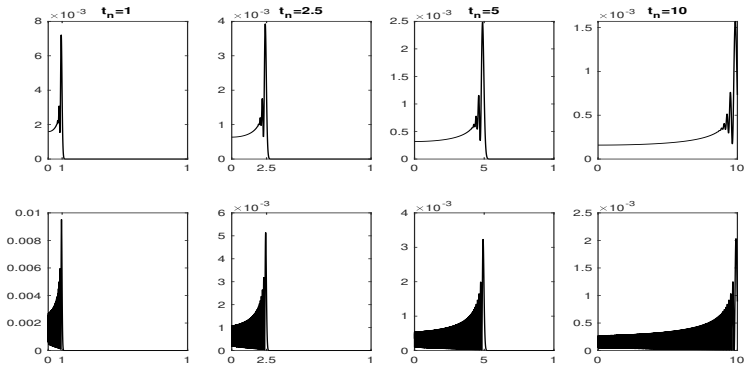

FIG. 1. *Wave equation without damping ($c = 1$, $\alpha = 0$). Behavior of the coefficients $\omega_n^{\mathcal{V}}(r; \Delta t)$ with respect to r, for $\Delta t = 1.0e - 02$ for the BDF2 (top row) and the TRAP (bottom row) rule.*

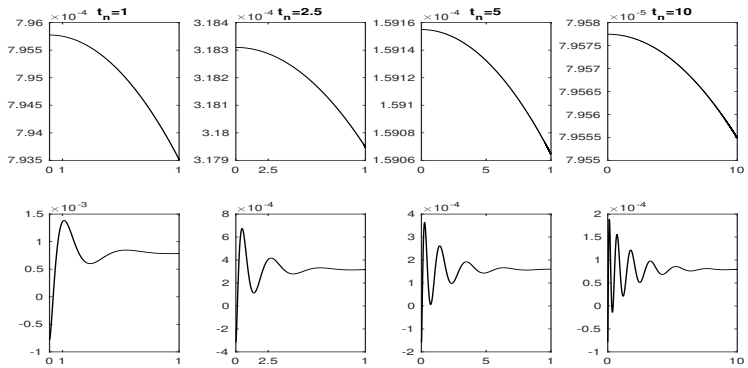

FIG. 2. *Wave equation with damping: silicon ($c = 9685 \cdot m/s$ and $\alpha = 1.1 \times 10^4 \cdot m^2/s$). Behavior of the coefficients $\omega_n^{\mathcal{V}}(r; \Delta t)$ with respect to r, for $\Delta t = 1.0e - 02$, for the BDF2 (top row) and the TRAP (bottom row) rule.*

of the presence of the damping parameter α, no tails are present but, again, the coefficients, when the BDF2 and TRAP rules are considered, display a very different behavior.

As we will see in section 5, the behavior of $\omega_n^{\mathcal{J}}(r; \Delta t)$ affects the compression property of the wavelet approach. In particular, the regularity of the tail of $\omega_n^{\mathcal{J}}(r; \Delta t)$ influences the choice of a wavelet basis, with a suitable number of vanishing moments, to retrieve a high compression of the wavelet BEM matrices. Without going into detail, we recall that the number $\bar{m}$ of vanishing moments of a wavelet corresponds to the orthogonality property between the wavelet basis functions and polynomials of degree less than or equal to $\bar{m} - 1$, a property that has an effect on the matrix compression [14]. Hence, the smoother the tail of $\omega_n^{\mathcal{J}}(r; \Delta t)$, the lower the number $\bar{m}$ of the wavelet vanishing moments can be chosen; vice versa, the presence of high oscillations in the tails will enforce choosing wavelets with a higher number of vanishing moments.

3.2. Space discretization: Galerkin method. For the space discretization we will employ a Galerkin wavelet BEM. To this aim we start by introducing the Galerkin BEM based on Lagrangian functions (standard case). For simplicity, we assume that the curve Γ is given by either a global or a piecewise (local) parametric

representation, including the cases of both smooth and nonregular (polygonal) boundaries. We remark that the sparsification property of the BEM matrices in terms of the wavelet bases does not depend on the regularity of Γ.

For ease of presentation we consider the case of a global parametrization given by $\mathbf{x} := \boldsymbol{\xi}(\sigma) = (\xi_1(\sigma), \xi_2(\sigma))$ and $\mathbf{y} := \boldsymbol{\xi}(\theta) = (\xi_1(\theta), \xi_2(\theta))$ with $\sigma, \theta \in (-\pi, \pi]$. In this case, the integration over Γ is reduced to an equivalent integration over the parametrization interval $(-\pi, \pi]$. We introduce a uniform partition $\mathcal{E}$ of this interval, consisting of M elements e_i of width $\Delta\theta = {}^{2\pi}/_{M}$, $i = 1, \ldots, M$. Denoting by $\mathcal{P}_1$ the space of univariate polynomials of maximal degree 1, we introduce the space

$$X^{1,1}_{\Delta\theta} := \{\widetilde{\psi} = (\psi \circ \boldsymbol{\xi}^{-1}) \in L^2(\Gamma) \ : \psi_{|e_i} \in \mathcal{P}_1 \ \forall\, e_i \in \mathcal{E}\} \cap H^1(\Gamma) \tag{3.8}$$

of piecewise linear functions associated to the partition $\mathcal{E}$. Let $\{N_i(\theta)\}_{i=1}^{M+1}$ denote the classical Lagrangian basis functions associated with the nodes $\{\theta_i\}_{i=1}^{M+1}$ of $\mathcal{E}$, i.e., $N_i(\theta_k) = \delta_{ik}$. This defines the associated interpolant of $\varphi_j(\mathbf{y})$ on the curve Γ:

$$\varphi_j(\xi(\theta)) \simeq \varphi_j^{\Delta\theta}(\theta) := \sum_{i=1}^{M+1} \varphi_j^i N_i(\theta) \qquad \forall j = 0, \ldots, N. \tag{3.9}$$

Taking into account that Γ is a closed curve, it results in $\varphi_j^1 = \varphi_j^{M+1}$.

In the case of a boundary condition of Dirichlet type, the discrete problem consists of finding the coefficients φ_j^i such that

$$\begin{aligned} &\sum_{j=0}^{n} \sum_{i=1}^{M} \varphi_j^i \int_{-\pi}^{\pi} \int_{-\pi}^{\pi} \omega^{\mathcal{V}}_{n-j}(r; \Delta t) N_i(\theta) N_m(\sigma) |\boldsymbol{\xi}'(\theta)| |\boldsymbol{\xi}'(\sigma)| d\theta d\sigma \\ &\quad = \int_{-\pi}^{\pi} f_n(\boldsymbol{\xi}(\sigma)) N_m(\sigma) |\boldsymbol{\xi}'(\sigma)| d\sigma. \end{aligned} \tag{3.10}$$

In the case of a boundary condition of Neumann type, the discrete problem consists of finding the coefficients φ_j^i such that

$$\begin{aligned} &\frac{1}{2} \sum_{i=1}^{M} \varphi_j^i \int_{-\pi}^{\pi} N_i(\sigma) N_m(\sigma) |\boldsymbol{\xi}'(\sigma)| d\sigma \\ &\qquad - \sum_{i=1}^{M} \sum_{j=0}^{n} \varphi_j^i \int_{-\pi}^{\pi} \int_{-\pi}^{\pi} \omega^{\mathcal{K}}_{n-j}(r; \Delta t) N_i(\theta) N_m(\sigma) |\boldsymbol{\xi}'(\theta)| |\boldsymbol{\xi}'(\sigma)| d\theta d\sigma \\ &\quad = \int_{-\pi}^{\pi} g_n(\boldsymbol{\xi}(\sigma)) N_m(\sigma) |\boldsymbol{\xi}'(\sigma)| d\sigma. \end{aligned} \tag{3.11}$$

Both (3.10) and (3.11) are to be considered for $n = 0, \ldots, N$ and $m = 1, \ldots, M$. The matrix representation of (3.10) is

$$\mathbb{V}^0 \boldsymbol{\varphi}_n = \boldsymbol{f}_n - \sum_{j=0}^{n-1} \mathbb{V}^{n-j} \boldsymbol{\varphi}_j, \qquad n = 0, \ldots, N, \tag{3.12}$$

while that of (3.11) is

$$\left(\frac{1}{2}\mathbb{M} - \mathbb{K}^0\right) \boldsymbol{\varphi}_n = \boldsymbol{g}_n + \sum_{j=0}^{n-1} \mathbb{K}^{n-j} \boldsymbol{\varphi}_j, \qquad n = 0, \ldots, N. \tag{3.13}$$

In the linear systems (3.12) and (3.13), the unknown vectors are $\boldsymbol{\varphi}_j = (\varphi_j^1, \ldots, \varphi_j^M)^\top$, the generic elements of the matrices $\mathbb{V}^n$ and $\mathbb{K}^n$ are

(3.14)
$$\mathbb{V}^n_{i,m} := \int_{-\pi}^{\pi}\int_{-\pi}^{\pi} \omega_n^{\mathcal{V}}(r;\Delta t) N_i(\theta) N_m(\sigma) |\boldsymbol{\xi}'(\theta)||\boldsymbol{\xi}'(\sigma)| d\theta d\sigma, \qquad i,m = 1,\ldots,M,$$

(3.15)
$$\mathbb{K}^n_{i,m} := \int_{-\pi}^{\pi}\int_{-\pi}^{\pi} \omega_n^{\mathcal{K}}(r;\Delta t) N_i(\theta) N_m(\sigma) |\boldsymbol{\xi}'(\theta)||\boldsymbol{\xi}'(\sigma)| d\theta d\sigma, \qquad i,m = 1,\ldots,M,$$

and the components of the RHS vectors $\boldsymbol{f}_n$ and $\boldsymbol{g}_n$ are given by

$$f_n^m := \int_{-\pi}^{\pi} f_n(\boldsymbol{\xi}(\sigma)) N_m(\sigma) |\boldsymbol{\xi}'(\sigma)| d\sigma \quad \text{and} \quad g_n^m := \int_{-\pi}^{\pi} g_n(\boldsymbol{\xi}(\sigma)) N_m(\sigma) |\boldsymbol{\xi}'(\sigma)| d\sigma,$$

for $m = 1, \ldots, M$.
In (3.13), $\mathbb{M}$ stands for the standard mass matrix, whose entry of index i,m is

$$\mathbb{M}_{i,m} := \int_{-\pi}^{\pi} N_i(\sigma) N_m(\sigma) |\boldsymbol{\xi}'(\sigma)| d\sigma.$$

By combining (3.14) and (3.15) with (3.7), the elements of matrices $\mathbb{V}^n$ and $\mathbb{K}^n$ can be recast as

$$\mathbb{V}^n_{i,m} \simeq \frac{\varrho^{-n}}{\tilde{R}} \sum_{l=0}^{\tilde{R}-1} \mathbb{C}^{\mathcal{V}}_{i,m}(l) e^{-\imath n l \frac{2\pi}{\tilde{R}}} \qquad \text{and} \qquad \mathbb{K}^n_{i,m} \simeq \frac{\varrho^{-n}}{\tilde{R}} \sum_{l=0}^{\tilde{R}-1} \mathbb{C}^{\mathcal{K}}_{i,m}(l) e^{-\imath n l \frac{2\pi}{\tilde{R}}}, \tag{3.16}$$

where

(3.17)
$$\mathbb{C}^{\mathcal{J}}_{i,m}(l) := \int_{-\pi}^{\pi}\int_{-\pi}^{\pi} \widehat{G}^{\mathcal{J}}\left(r; \frac{\gamma(\varrho e^{\imath l \frac{2\pi}{\tilde{R}}})}{\Delta t}\right) N_i(\theta) N_m(\sigma) |\boldsymbol{\xi}'(\theta)||\boldsymbol{\xi}'(\sigma)| d\theta d\sigma, \qquad \mathcal{J} = \{\mathcal{V}, \mathcal{K}\}.$$

Thus, the entries of index i,m of the matrices $\mathbb{V}^n$ and $\mathbb{K}^n$, for $n = 0, \ldots, N$, can be computed simultaneously by the FFT algorithm, with $\mathcal{O}(\tilde{R}\log\tilde{R})$ flops.

Remark 3.2. Assuming compatibility conditions on the initial and boundary data [21, 22], since $\mathbb{V}^0$ and $\mathbb{K}^0$ are nonsingular, we have $\boldsymbol{\varphi}_0 = 0$. Therefore, the linear systems (3.12) and (3.13) are iteratively solved for $n = 1, \ldots, N$.

4. Fast wavelet based CQ-BEM. There are basically two strategies for applying the wavelet technique to CQ-BEM: a *direct* strategy which consists in generating the BEM matrices by expanding the unknown density function $\varphi(\mathbf{x};t)$ in terms of the wavelet basis, and an *indirect* strategy which applies a wavelet transform to the BEM matrices obtained by expanding the unknown function in terms of standard piece-wise linear nodal basis functions. We remark that both approaches allow us to preserve the use of the FFT algorithm and its benefits for the construction of the matrices; see [14].

The *direct* strategy, presented in [14] for the wave equation, allows us to apply an a priori matrix compression, by computing only the significant entries of the matrices involved in the final linear system, thus reducing both the global computational cost and the memory space. This method, which is based on the a priori knowledge of the behavior in time of the matrix entries, has been designed for the particular choice

of the biorthogonal BIOR2.2 wavelets. Moreover, the approach requires some ad hoc quadrature strategies to compute the matrix entries with a high accuracy, a key issue for the success of the CQ method that has not been deeply investigated yet in the wavelet context. In view of the above considerations, if a higher order wavelet basis is needed to obtain a major compression (see Remark 3.1), an accurate quadrature rule may become demanding, or even impossible when, for example, wavelets are not given in analytic form. In [20, 33, 34, 35, 36] wavelet based compression strategies and efficient quadratures have been proposed and applied to several 2D and 3D BEM. All the mentioned works deal with time independent problems, including Helmholtz ones, and the numerical results therein presented are obtained with piecewise constant or piecewise linear wavelets. Since the sparsity pattern of the wavelet BEM matrices varies in time (as shown in [14] for the particular choice of the BIOR2.2), the compression strategies proposed in the above-mentioned papers can be in principle applied only at each time instant, disregarding the use of the FFT during the construction of the matrices. Alternatively, as suggested in [7], an equivalent system of Helmholtz problems associated to different wave numbers could be considered as well, and the wavelet sparsification technique could be applied to each Helmholtz matrix in association to an FFT based solver. This strategy was revealed to be particularly efficient when, under suitable assumptions on the problem data, only a few Helmholtz matrices must be computed and stored. Since the aim of our approach is to retrieve the temporal history of each entry of the matrices via the FFT, and to solve generic time dependent problems, we will not apply such strategies.

The *indirect* strategy is purely numerical and allows us to obtain a compression by setting equal to zero all the matrix entries which are negligible up to a given threshold parameter $\varepsilon > 0$. In this second case, the a priori storage of all the matrices is needed, and the memory saving is obtained only a posteriori, as shown in [14].

In this work we propose a new strategy, based on a purely numerical procedure, that allows us to benefit both from the FFT in the CQ-BEM and from the wavelet compression, by the application of the DWT. We recall that the DWT is a fast algorithm that allows us to perform a change of basis, that in our case is from the standard piecewise linear nodal basis functions into a wavelet basis. The use of the DWT will allow us to obtain accurate wavelet BEM matrix entries, independently of the choice of the wavelet basis, through an accurate computation of the integrals associated to the Lagrangian basis, the latter being a well-established task [21, 22]. Moreover, we will see that the new procedure allows us to store only the matrix entries which are significant up to a prescribed tolerance, without the need for storing a priori all the fully populated matrices associated to the use of the Lagrangian basis for the space discretization.

4.1. A new DWT based compression technique for CQ-BEM. Let us introduce the square matrix $\mathbb{W}$, whose columns store the wavelet decomposition of the piecewise linear basis functions at the level L, this latter being associated to the refinement of the parametrization interval $(-\pi, \pi]$ of Γ by the relation $M = 2^L$. By rewriting (3.12) and (3.13) as

$$\mathbb{V}^0(\mathbb{W}^{-1}\mathbb{W})\boldsymbol{\varphi}_n = \boldsymbol{f}_n - \sum_{j=0}^{n-1} \mathbb{V}^{n-j}(\mathbb{W}^{-1}\mathbb{W})\boldsymbol{\varphi}_j, \qquad n = 1, \dots, N, \tag{4.1}$$

$$\left(\frac{1}{2}\mathbb{M} - \mathbb{K}^0\right)(\mathbb{W}^{-1}\mathbb{W})\boldsymbol{\varphi}_n = \boldsymbol{g}_n + \sum_{j=0}^{n-1} \mathbb{K}^{n-j}(\mathbb{W}^{-1}\mathbb{W})\boldsymbol{\varphi}_j, \qquad n = 1, \dots, N, \tag{4.2}$$

the standard wavelet Galerkin method is obtained by premultiplying the previous equations by $\mathbb{W}^{-\top}$, thus getting

(4.3)
$$\mathbb{V}^{\mathcal{W},0}\boldsymbol{\varphi}_n^{\mathcal{W}} = \boldsymbol{f}_n^{\mathcal{W}} - \sum_{j=0}^{n-1} \mathbb{V}^{\mathcal{W},n-j}\boldsymbol{\varphi}_j^{\mathcal{W}} \quad \text{and} \quad \mathbb{K}^{\mathcal{W},0}\boldsymbol{\varphi}_n^{\mathcal{W}} = \boldsymbol{g}_n^{\mathcal{W}} + \sum_{j=0}^{n-1} \mathbb{K}^{\mathcal{W},n-j}\boldsymbol{\varphi}_j^{\mathcal{W}},$$

for $n = 1, \ldots, N$, with $\mathbb{V}^{\mathcal{W},j} = \mathbb{W}^{-\top}\mathbb{V}^j\mathbb{W}^{-1}$, $\mathbb{K}^{\mathcal{W},j} = \mathbb{W}^{-\top}\mathbb{K}^j\mathbb{W}^{-1}$, $\boldsymbol{f}_n^{\mathcal{W}} := \mathbb{W}^{-\top}\boldsymbol{f}_n$, and $\boldsymbol{g}_n^{\mathcal{W}} := \mathbb{W}^{-\top}\boldsymbol{g}_n$.

We observe that when orthogonal wavelets are used, like, for example, the Daubechies ones, it results in $\mathbb{W}^{-1} = \mathbb{W}^{\top}$ so that no matrix inversion is required. With reference to formulas (3.16) and (3.17), we describe the main issues relative to the implementation of the *indirect* CQ-BEM wavelet approach to retrieve the matrices $\mathbb{V}^{\mathcal{W},j}$ (and $\mathbb{K}^{\mathcal{W},j}$), based on the DWT and the a posteriori compression strategy. These are summarized in the following steps:

Indirect CQ-BEM algorithm:

1. for all the values of the row and column indices i and m
   (a) compute the entries $\mathbb{C}_{i,m}^{\mathcal{V}}(l)$, for all values $l = 0, 1, \ldots, \tilde{R} - 1$, by applying a ν-point Gauss–Legendre rule (see [21] and [23]);
   (b) compute the vector $\mathcal{F}$, of $\tilde{R}$ components, defined as $\mathcal{F} := \mathrm{FFT}\left(\mathbb{C}_{i,m}^{\mathcal{V}}\right)$;
   (c) retrieve the matrix entries $\mathbb{V}_{i,m}^{n} = \frac{\varrho^{-n}}{\tilde{R}}\,\mathcal{F}(n)$ for $n = 0, \ldots, N$;
2. for all $n = 0, \ldots, N$
   (a) compute $\mathbb{V}^{\mathcal{W},n} := \mathbb{W}^{-\top}\mathbb{V}^n\mathbb{W}^{-1}$;
   (b) sparsify

$$\mathbb{V}_{i,m}^{\mathcal{W},n} := \begin{cases} \mathbb{V}_{i,m}^{\mathcal{W},n} & \text{if } |\mathbb{V}_{i,m}^{\mathcal{W},n}| > \varepsilon, \\ 0 & \text{otherwise} \end{cases} \qquad \text{for } i, m = 1, \ldots, M. \tag{4.4}$$

In formula (4.4), by abuse of notation, we have denoted with the same symbol the matrices before and after the compression. Moreover, we remark that, after step 1(c), we have stored all the matrix entries associated to all the time instants. To avoid such a drawback, we propose a new strategy by preliminarily observing that the entry of index i, m of $\mathbb{V}^{\mathcal{W},n}$ is given by

$$\mathbb{V}_{i,m}^{\mathcal{W},n} = \sum_{h=1}^{M} \mathbb{W}_{i,h}^{-\top}\widetilde{\mathbb{V}}_{h,m}^{\mathcal{W},n} := \sum_{h=1}^{M} \mathbb{W}_{i,h}^{-\top}\left(\sum_{k=1}^{M} \mathbb{V}_{h,k}^{n}\mathbb{W}_{k,m}^{-1}\right). \tag{4.5}$$

According to (3.16), and by taking advantage of the linearity property of the FFT, we can rewrite (4.5) as follows:

$$\begin{aligned} \mathbb{V}_{i,m}^{\mathcal{W},n} &\simeq \sum_{h=1}^{M} \mathbb{W}_{i,h}^{-\top}\left(\frac{\varrho^{-n}}{\tilde{R}} \sum_{l=0}^{\tilde{R}-1}\sum_{k=1}^{M} \mathbb{C}_{h,k}^{\mathcal{V}}(l)\mathbb{W}_{k,m}^{-1} e^{-\imath n l \frac{2\pi}{\tilde{R}}}\right) \\ &:= \sum_{h=1}^{M} \mathbb{W}_{i,h}^{-\top}\left(\frac{\varrho^{-n}}{\tilde{R}} \sum_{l=0}^{\tilde{R}-1} \widetilde{\mathbb{C}}_{h,m}^{\mathcal{V}}(l) e^{-\imath n l \frac{2\pi}{\tilde{R}}}\right), \end{aligned} \tag{4.6}$$

where the coefficients $\widetilde{\mathbb{C}}^{\mathcal{V}}_{h,m}$ are

$$\widetilde{\mathbb{C}}^{\mathcal{V}}_{h,m}(l) := \int_{-\pi}^{\pi}\int_{-\pi}^{\pi} \widehat{G}^{\mathcal{J}}\left(r; \frac{\gamma\left(\varrho e^{il\frac{2\pi}{\tilde{R}}}\right)}{\Delta t}\right) N_h(\theta)\psi_m(\sigma)|\boldsymbol{\xi}'(\theta)||\boldsymbol{\xi}'(\sigma)|d\theta d\sigma.$$

In the above equation, we have denoted by $\boldsymbol{\psi} = \{\psi_m\}_{m=1}^M$ the set of wavelet basis functions, retrieved from the set of the Lagrangian basis $\boldsymbol{N} = \{N_m\}_{m=1}^M$ by the relation $\boldsymbol{\psi} = \mathbb{W}^{-1}\mathbf{N}$. Moreover note that, at this stage, the entries of the matrices $\widetilde{\mathbb{V}}^{\mathcal{W},j}$ and $\widetilde{\mathbb{K}}^{\mathcal{W},j}$ are not those associated to the standard wavelet Galerkin scheme. They are associated to a Petrov–Galerkin approach where the trial space is that spanned by the wavelet basis functions, while the test space is that of the nodal piecewise linear basis functions.

The main steps relative to the implementation of this new CQ-BEM wavelet approach to retrieve the matrices $\mathbb{V}^{\mathcal{W},j}$ (and $\mathbb{K}^{\mathcal{W},j}$) are as follows:

New CQ-BEM algorithm:

1. for each value of the row index $h = 1, \ldots, M$,
   (a) compute the whole hth row $\mathbb{C}^{\mathcal{V}}_{h,\cdot}(l)$ for all $l = 0, 1, \ldots, \tilde{R} - 1$;
   (b) compute the whole hth row $\widetilde{\mathbb{C}}^{\mathcal{V}}_{h,\cdot}(l) = \sum_{k=0}^{M} \mathbb{C}^{\mathcal{V}}_{h,k}(l)\mathbb{W}^{-1}_{k,\cdot}$ for all $l = 0, 1, \ldots, \tilde{R} - 1$;
   (c) compute the vector $\widetilde{\mathcal{F}}$, of $\tilde{R}$ components, defined as $\widetilde{\mathcal{F}} := \mathrm{FFT}\left(\widetilde{\mathbb{C}}^{\mathcal{V}}_{i,\cdot}\right)$;
   (d) retrieve the matrix entries $\widetilde{\mathbb{V}}^{\mathcal{W},n}_{h,\cdot} = \frac{\varrho^{-n}}{\tilde{R}}\,\widetilde{\mathcal{F}}(n)$ for $n = 0, \ldots, N$;
   (e) sparsify

$$\widetilde{\mathbb{V}}^{\mathcal{W},n}_{h,m} := \begin{cases} \widetilde{\mathbb{V}}^{\mathcal{W},n}_{h,m} & \text{if } |\widetilde{\mathbb{V}}^{\mathcal{W},n}_{h,m}| > \varepsilon, \\ 0 & \text{otherwise} \end{cases} \qquad \text{for } m = 1, \ldots, M,\ n = 0, \ldots, N. \tag{4.7}$$

2. for all $n = 0, \ldots, N$
   (a) compute $\mathbb{V}^{\mathcal{W},n} := \mathbb{W}^{-\top}\widetilde{\mathbb{V}}^{\mathcal{W},n}$;
   (b) sparsify

$$\mathbb{V}^{\mathcal{W},n}_{i,m} := \begin{cases} \mathbb{V}^{\mathcal{W},n}_{i,m} & \text{if } |\mathbb{V}^{\mathcal{W},n}_{i,m}| > \varepsilon, \\ 0 & \text{otherwise} \end{cases} \qquad \text{for } i, m = 1, \ldots, M. \tag{4.8}$$

Once again, in formulas (4.7)–(4.8), by abuse of notation, we have denoted with the same symbol the matrices before and after the compression.

Remark 4.1. We remark that the success of the new proposed scheme relies on the possibility of obtaining sparse matrices $\widetilde{\mathbb{V}}^{\mathcal{W},n}$ and $\widetilde{\mathbb{K}}^{\mathcal{W},n}$, for $n = 0, \ldots, N$, after having performed the first step (4.7) of the compression strategy. To show indeed the effectiveness of the sparsification technique, we consider as a benchmark example the wave equation without damping, i.e., $c = 1 \cdot \mathrm{m/s}$ and $\alpha = 0 \cdot \mathrm{m^2/s}$. The domain Ω is the unit disk centered at $(0, 0)$, so that $\Gamma := \{\mathbf{x} \in \mathbf{R}^2 \ : \ \mathbf{x} = (\cos\theta, \sin\theta),\ \theta \in (-\pi, \pi]\}$, and the parametrization interval $(-\pi, \pi]$ is decomposed into $M = 2^9$ $(L = 9)$ subintervals. The final time instant is set $T = 10$ and time interval of interest $[0, 10]$ is subdivided into $N = 1000$ subintervals. We apply a BDF2 CQ-wavelet BEM by choosing the BIOR2.2 and Daubechies DB45 wavelet basis (see Figure 3).

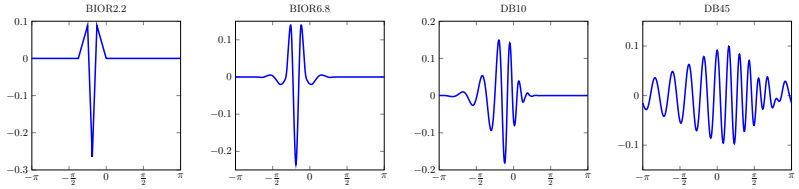

FIG. 3. *Behavior of the reconstruction wavelet functions* $\psi_{4,6}$ *associated to BIOR*2.2*, BIOR*6.8*, DB*10*, and DB*45*, for* $L = 9$*. We refer to* [14] *for details on the wavelet multi-index notation and its relation with the standard index set* $\{1, \dots, M\}$*.*

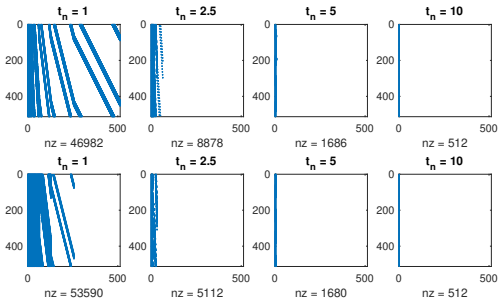

FIG. 4. *Wave equation without damping* ($c = 1 \cdot m/s$ *and* $\alpha = 0 \cdot m^2/s$)*. Sparsity pattern of* $\tilde{\mathbb{V}}^{\mathcal{W},n}$ *with BIOR*2.2 *(top row) and* $\tilde{\mathbb{V}}^{\mathcal{W},n}$ *with DB*45 *(bottom row), for the BDF*2 *rule and for* $n = 100, 250, 500, 1000$*.*

In Figure 4, we plot the sparsity pattern of the matrices $\widetilde{\mathbb{V}}^{\mathcal{W},n}$, for $n = 100, 250, 500, 1000$, by fixing the threshold $\varepsilon = 1.0e-08$ (biorthogonal BIOR2.2, top row, and Daubechies DB45, bottom row). Similar patterns have been obtained for the matrices $\widetilde{\mathbb{K}}^{\mathcal{W},n}$ and when damping terms have been considered. As we can see, after the first step of the compression strategy the BEM matrices are already highly sparse and, for increasing time, the nonzero entries gather toward the first columns, as an effect of the right multiplication of the BEM matrices $\mathbb{V}^n$ by the matrix $\mathbb{W}^{-1}$. We remark that the nonzero entries are the only ones actually stored before proceeding with the second compression. After the first step, it results that the percentage of memory saving is 95.75% for BIOR2.2 and 95.22% for Daubechies DB45. At the end of the complete compression process we get a total memory saving of 97.73% and 99.16% for the former and latter wavelet bases, respectively. Finally, we remark that we can use standard routines for sparse matrix/vector product to reduce the CPU time for the computation of the matrices $\mathbb{V}^{\mathcal{W},n}$ in step 2(a).

5. Numerical results. This section consists of two main parts: the first is devoted to the numerical study of the efficiency of the proposed method, in terms of memory saving and accuracy; the second presents the application of the scheme to some realistic problems.

In all the simulations presented, the CQ parameters are such that for a fixed η, the choice $\varrho^N = \sqrt{\eta}$ and $\tilde{R} = 2N$ allows us to compute the approximation of $\omega_n^{\mathcal{J}}$ with a relative error of order $\sqrt{\eta}$ if $\widehat{G}^{\mathcal{J}}$ is computed with a relative accuracy bounded by η. In particular, we have chosen $\eta = 1.0E-10$. The integrals over the boundary Γ, which define the matrix elements $\mathbb{V}_{i,m}^n$ and $\mathbb{K}_{i,m}^n$, for $n = 0, \dots, N$ (see (3.14)–(3.15)), are computed by using an 8-point (extra diagonal elements) and a 16-point (diagonal elements) Gauss–Legendre quadrature rule.

All the numerical computations have been run on a PC with Intel Core i7-7700 (3.60 GHz). To perform the numerical testing we have written standard (i.e., sequential) MATLAB codes.

5.1. Study of the complexity and of the accuracy of the new scheme. The efficiency of the global compression technique by the approach discussed in the previous section depends on the possible storage reduction obtained by the wavelet compression, whose direct consequence is an acceleration of the classical matrix/vector product, needed to update the RHS of (3.12) and (3.13) at each time step. In this section we present an accurate numerical study, aiming at showing the performance and the accuracy of the wavelet CQ-BEM. Precisely, in section 5.1.1 we report the numerical study of the global memory storage required by both the standard and the wavelet method, with respect to the space and time mesh refinement. In section 5.1.2 we show the sparsity pattern of the matrices associated to the two approaches at fixed time steps. Finally, in section 5.1.3, we study the behavior of the L^2 error of the solution of the BEM problems and we report the global convergence rate with respect to the space and time refinement.

As a benchmark example, in what follows the domain Ω is the unit disk centered at $(0,0)$, so that $\Gamma := \{\mathbf{x} \in \mathbf{R}^2 \ : \ \mathbf{x} = (\cos\theta, \sin\theta),\ \theta \in (-\pi, \pi]\}$. By varying the physical properties of Ω^e, we observe the dependency on c and α of the sparsity of the discrete integral operators. We fix the final time instant $T = 10$ and we consider two sets of physical parameters: $c = 1 \cdot {}^{\mathrm{m}}/_{\mathrm{s}}$ and $\alpha = 0 \cdot {}^{\mathrm{m}^2}/_{\mathrm{s}}$ (wave equation without damping), and $c = 9685 \cdot {}^{\mathrm{m}}/_{\mathrm{s}}$ and $\alpha = 1.1 \times 10^4 \cdot {}^{\mathrm{m}^2}/_{\mathrm{s}}$ (silicon; see [42]). As the wavelet basis, we use the biorthogonal BIOR2.2 and BIOR6.8 compactly supported wavelet functions [17] and the orthogonal Daubechies DB10 and DB45 compactly supported wavelet functions [18] (see Figure 3 for some basis functions associated to the level $L = 9$).

5.1.1. Storage requirement. In this first numerical investigation, we compare the computed storage requirement of the wavelet approach with that needed by the full matrix representation, which is $\mathcal{O}(M^2)$ for each matrix of the time marching and $\mathcal{O}(NM^2)$ globally. We consider the CQ-wavelet BEM with both the BDF2 (Figure 5) and TRAP (Figure 6) ODE solvers and we fix the threshold $\varepsilon = 1.0E-12$, which ensures that the accuracy of the solution of the problem is not affected by the compression of the system matrices, as we are going to show in section 5.1.3. We study

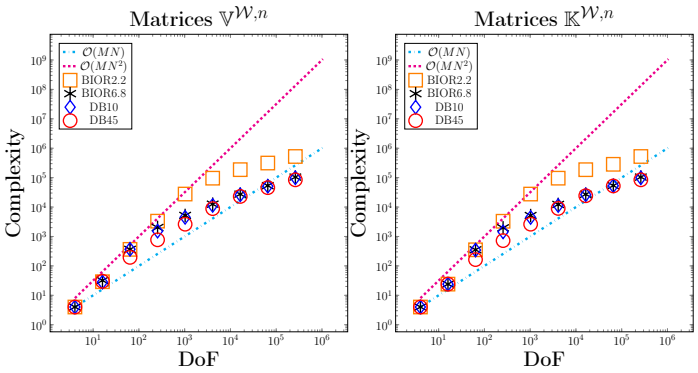

FIG. 5. *Silicon ($c = 9685 \cdot {}^{m}/_{s}$ and $\alpha = 1.1 \times 10^4 \cdot {}^{m^2}/_{s}$). Comparison of the complexity for the BIOR2.2, BIOR6.8, DB10, and DB45 wavelet based compression ($\varepsilon = 1.0E-12$) for the matrices $\mathbb{V}^{\mathcal{W},n}$ (left plot) and $\mathbb{K}^{\mathcal{W},n}$ (right plot) for the BDF2 ODE solver.*

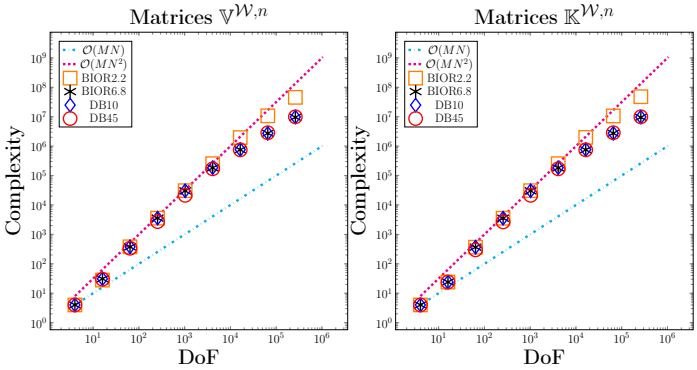

FIG. 6. *Silicon ($c = 9685 \cdot m/s$ and $\alpha = 1.1 \times 10^4 \cdot m^2/s$). Comparison of the complexity for the BIOR2.2, BIOR6.8, DB10, and DB45 wavelet based compression ($\varepsilon = 1.0E-12$) for the matrices $\mathbb{V}^{\mathcal{W},n}$ (left plot) and $\mathbb{K}^{\mathcal{W},n}$ (right plot) for the TRAP ODE solver.*

the complexity of the proposed method for an increasing number of degrees of freedom (DoF), i.e., for increasing values of MN; in particular we choose $M = N = 2^L$, $L = 1, \ldots, 9$. When α is small compared to c, as in the case of silicon, we underline that the growth is less than linear $\mathcal{O}(NM)$ for the BDF2 solver (see Figure 5), while it tends to be linear in the case of the TRAP rule (see Figure 6). On the other hand, in the case of the standard wave equation (or when α is big compared to c), we have obtained the same linear complexity growth as in [14] for both the BDF2 and TRAP solvers. Therefore, we omit the corresponding graphs. In all the tested cases, no substantial differences are observed for the compression of the matrices $\mathbb{V}^{\mathcal{W},n}$ and $\mathbb{K}^{\mathcal{W},n}$ for $n = 0, \ldots, N$. As we expect, the use of the BIOR6.8 and DB45 wavelets is more efficient than BIOR2.2 and DB10, in terms of matrix compression, because the former bases have a larger number of vanishing moments. Finally, we remark that the BIOR6.8 and DB10 wavelet functions approximately give the same memory saving.

5.1.2. Sparsity pattern of the BEM matrices. We consider a decomposition of the parametric interval $(-\pi, \pi]$ in $M = 2^9$ subintervals and we subdivide the time interval of interest $[0, 10]$ into $N = 1000$ subintervals. We compare the results of the proposed wavelet compression technique (approach $\mathcal{W}$) with those obtained by using a *standard* compression (approach $\mathcal{S}$), consisting of an a posteriori cutting, obtained by setting equal to zero the entries of the matrices $\mathbb{V}^n$ which are, in absolute value, less than or equal to ε. In what follows we will denote by $\mathbb{V}^{*,n}$, $* = \{\mathcal{S}, \mathcal{W}\}$ the matrices corresponding to the approaches $\mathcal{S}$ and $\mathcal{W}$, respectively. We fix $\varepsilon = 1.0E-08$ for both the approach $\mathcal{S}$ and the approach $\mathcal{W}$. For the analysis of the sparsity patterns of the matrices $\mathbb{V}^{*,n}$ for $n = 100, 250, 500, 1000$, we consider the TRAP and BDF2 ODE solvers.

In the case of the wave equation without damping (Figure 7), at the time instant $t_n = 1$ the compressed matrix generated by the standard technique is sparse, while for the other instants it is fully populated for both the BDF2 and TRAP rules. We note that the wavelet compression is very efficient when the BDF2 rule is considered, since very few entries of the system matrices are stored. On the other hand, when we use the TRAP solver, the compressed matrices with BIOR2.2 wavelets rule have the typical finger structure at all the time instants, while in the case of DB45 wavelets only the first two matrices have the finger structure and the others are even sparser. We

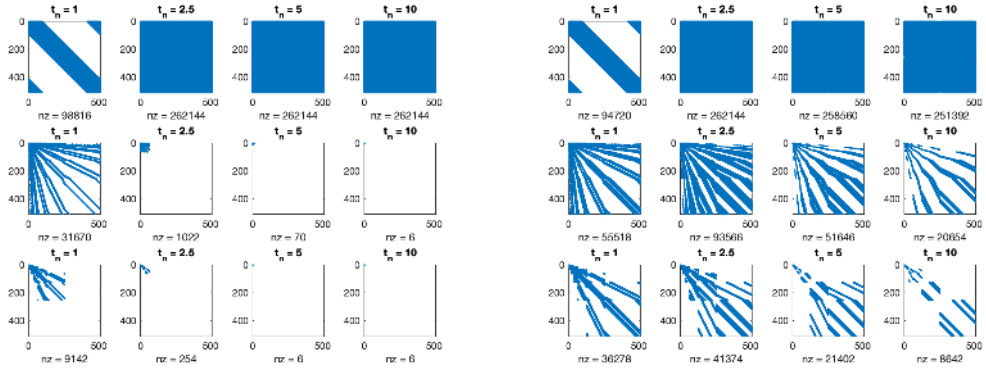

(a) BDF2 rule (b) TRAP rule

FIG. 7. *Wave equation without damping ($c = 1 \cdot m/s$ and $\alpha = 0 \cdot m^2/s$). Sparsity pattern of $\mathbb{V}^{\mathcal{S},n}$ (top row), $\mathbb{V}^{\mathcal{W},n}$ with BIOR2.2 (middle row), and $\mathbb{V}^{\mathcal{W},n}$ with DB45 (bottom row) at t_n for BDF2 and TRAP rules.*

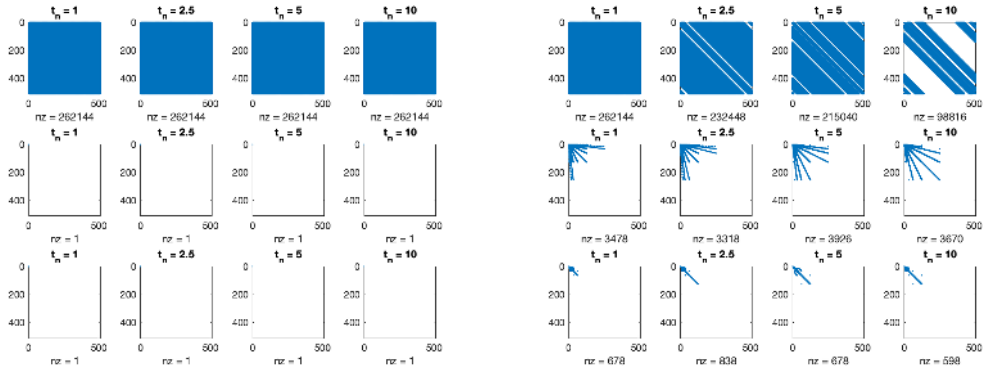

(a) BDF2 rule (b) TRAP rule

FIG. 8. *Silicon ($c = 9685 \cdot m/s$ and $\alpha = 1.1 \times 10^4 \cdot m^2/s$). Sparsity pattern of $\mathbb{V}^{\mathcal{S},n}$ (top row), $\mathbb{V}^{\mathcal{W},n}$ with BIOR2.2 (middle row) and $\mathbb{V}^{\mathcal{W},n}$ with DB45 (bottom row) at t_n for BDF2 and TRAP rules.*

can conclude that the wavelet compression is stronger when applied to the matrices $\mathbb{V}^n$ obtained with the BFD2 rule, because the coefficients $\omega_n^{\mathcal{V}}(r;\Delta t)$ related to this ODE solver are less oscillatory than those related to the TRAP solver (see Figure 1).

If we consider the physical parameters of silicon (Figure 8), we remark how we do not have any advantage from the standard approach $\mathcal{S}$ since almost all the entries of the matrices, for all the time instants, are computed and stored with a consequently null memory saving and, hence, no acceleration in the computation of the RHS vectors. On the other hand, the effectiveness of the matrix compression is optimal for the approach $\mathcal{W}$. When the BDF2 rule is used, only a few nonzero matrix elements are maintained, due to the almost constant behavior of the coefficients $\omega_n^{\mathcal{V}}(r;\Delta t)$ depicted in Figure 2 (top row). When the TRAP rule is used, the coefficients $\omega_n^{\mathcal{V}}(r;\Delta t)$ are oscillatory (Figure 2, bottom row), and this behavior leads to the need for storing a larger number of matrix elements. In this case, the largest number of vanishing

moments of the DB45 wavelet basis ensures a better compression. Analogous results have been observed for the matrices $\mathbb{K}^{*,n}$ with $^* = \mathcal{S}, \mathcal{W}$.

5.1.3. Accuracy of the wavelet compression. We consider the exterior Dirichlet problem (2.1) with the datum $f(\mathbf{x};t) = t^4 e^{-t}\cos(x_1^2 + 2x_2^2)$.

Here, we aim at testing the accuracy and the efficiency of the approximations we obtain by using the CQ-BEM approach and the standard and wavelet based compression. Since an analytical expression of the exact solution of the problem is not known, we construct the corresponding reference solution by solving the problem with the standard CQ-BEM by using $M_e = 512$ subintervals for the discretization of the parametrization interval $(-\pi, \pi]$ and $N_e = 2048$ subintervals for the time interval $[0, 10]$. We refer to the reference solution as $\varphi_{M_e,N_e}(\mathbf{x};t)$ and to the corresponding potential function as $u_{M_e,N_e}(\mathbf{x};t)$. We denote by $\varphi_{M,N}(\mathbf{x};t)$ and $u_{M,N}(\mathbf{x};t)$ the approximate solution and the corresponding potential function obtained with the proposed wavelet based and standard compressions, choosing the space and time discretization parameters M and N, respectively.

To test the accuracy of our method, we introduce the relative errors at the final time instant T:

$$E_\varphi^{M,N} := \frac{\left\|\varphi_{M_e,N_e}(\cdot;T) - \varphi^*_{M,N}(\cdot;T)\right\|_{L^2(\Gamma)}}{\|\varphi_{M_e,N_e}(\cdot;T)\|_{L^2(\Gamma)}}, \tag{5.1}$$

$$E_u^{M,N} := \frac{|u_{M_e,N_e}(\mathbf{x};T) - u_{M,N}(\mathbf{x};T)|}{|u_{M_e,N_e}(\mathbf{x};T)|} \quad \text{for a fixed } \mathbf{x} \in \Omega^e, \tag{5.2}$$

associated to the approximate solutions $\varphi_{M,N}(\mathbf{x};t)$ and $u_{M,N}(\mathbf{x};t)$, respectively. In Tables 1 and 2, we report these quantities for the wavelet approach $\mathcal{W}$ that uses the BIOR2.2 wavelet basis functions and the corresponding estimated order of convergence (EOC), computed by using the standard formula

$$\text{EOC} := \log_2\left(\frac{E_\varphi^{M,N}}{E_\varphi^{2M,2N}}\right) \qquad \text{or} \qquad \text{EOC} := \log_2\left(\frac{E_u^{M,N}}{E_u^{2M,2N}}\right). \tag{5.3}$$

Additionally, we focus our attention on the percentage of the memory saving, defined as

$$\text{mem}^*(\%) := 100 \cdot \left(1 - \frac{\text{nz}}{M^2 N}\right) \qquad \text{with } * = \mathcal{S}, \mathcal{W}, \tag{5.4}$$

TABLE 1

Wave equation without damping ($c = 1 \cdot {}^m/_s$ and $\alpha = 0 \cdot {}^{m^2}/_s$). Errors, convergence orders, and memory saving for the standard, wavelet BIOR2.2, wavelet BIOR6.8, and wavelet DB45 compressions. $T = 10$.

						BDF2				TRAP			
M	N	$E_\varphi^{M,N}$	EOC	$E_u^{M,N}$	EOC	$\text{mem}^{\mathcal{S}}$	$\text{mem}^{\mathcal{W}}_{\text{BIOR2.2}}$	$\text{mem}^{\mathcal{W}}_{\text{BIOR6.8}}$	$\text{mem}^{\mathcal{W}}_{\text{DB45}}$	$\text{mem}^{\mathcal{S}}$	$\text{mem}^{\mathcal{W}}_{\text{BIOR2.2}}$	$\text{mem}^{\mathcal{W}}_{\text{BIOR6.8}}$	$\text{mem}^{\mathcal{W}}_{\text{DB45}}$
8	32	1.15E − 01		7.40E − 03		0.0%	28.1%	28.1%	32.0%	0.0%	28.1%	28.1%	29.1%
			2.1		2.3								
16	64	2.71E − 02		1.50E − 03		0.0%	13.3%	13.3%	29.6%	0.5%	13.3%	13.3%	22.0%
			2.0		2.2								
32	128	6.63E − 02		3.27E − 04		2.1%	6.9%	26.7%	52.0%	3.6%	7.3%	6.4%	21.0%
			2.0		2.1								
64	256	1.60E − 03		7.60E − 05		5.3%	6.6%	56.1%	67.2%	6.8%	6.6%	3.8%	23.7%
			2.1		2.1								
128	512	3.73E − 04		1.73E − 05		7.9%	36.4%	73.5%	78.5%	9.1%	8.1%	5.0%	30.6%
			2.3		2.4								
256	1024	7.69E − 05		3.36E − 06		9.9%	72.9%	85.2%	89.9%	10.6%	12.8%	12.0%	36.9%

TABLE 2
Silicon ($c = 9685 \cdot m/s$ and $\alpha = 1.1 \times 10^4 \cdot m^2/s$). Errors, convergence orders, and memory saving for the standard, wavelet BIOR2.2, wavelet BIOR6.8, and wavelet DB45 compressions. $T = 10$.

						BDF2				TRAP			
M	N	$E_\varphi^{M,N}$	EOC	$E_u^{M,N}$	EOC	$\text{mem}^{\mathcal{S}}$	$\text{mem}^{\mathcal{W}}_{\text{BIOR2.2}}$	$\text{mem}^{\mathcal{W}}_{\text{BIOR6.8}}$	$\text{mem}^{\mathcal{W}}_{\text{DB45}}$	$\text{mem}^{\mathcal{S}}$	$\text{mem}^{\mathcal{W}}_{\text{BIOR2.2}}$	$\text{mem}^{\mathcal{W}}_{\text{BIOR6.8}}$	$\text{mem}^{\mathcal{W}}_{\text{DB45}}$
8	32	2.58E − 01		4.47E − 04		0.0%	35.1%	34.7%	76.7%	0.0%	25.7%	25.6%	25.6%
			2.2		2.1								
16	64	5.54E − 02		1.05E − 04		0.0%	21.2%	67.4%	92.1%	0.0%	13.0%	12.9%	31.3%
			2.0		2.0								
32	128	1.35E − 02		2.53E − 05		0.0%	29.1%	91.9%	97.0%	0.0%	6.4%	6.4%	33.3%
			2.0		2.0								
64	256	3.30E − 03		6.16E − 06		0.0%	76.5%	97.9%	98.9%	0.0%	3.2%	24.2%	33.4%
			2.1		2.1								
128	512	7.89E − 04		1.45E − 06		0.0%	95.2%	99.5%	99.6%	0.0%	2.5%	50.9%	58.1%
			2.3		2.3								
256	1024	1.58E − 04		2.90E − 07		0.0%	99.1%	99.8%	99.9%	0.0%	18.0%	74.2%	77.4%

where M^2N is the total number of matrix elements of the standard CQ-BEM and nz is the number of the elements that are stored after the cutting.

We choose the threshold parameter $\varepsilon = 1.0E - 12$. We remark that we have obtained the same accuracy also for the choice of the wavelet bases BIOR6.8, DB10, and DB45 as well as for the standard approach $\mathcal{S}$. Therefore, we do not report the latter, but only the comparison of the five approaches in terms of memory saving.

As we expected, we observe a quadratic convergence rate for both the approximate density $\varphi_{M,N}(\mathbf{x};t)$ and potential $u_{M,N}(\mathbf{x};t)$ functions. This result is due to a convergence rate in time proportional to $\mathcal{O}(\Delta t^2)$, as forecast in [41], and a convergence rate in space proportional to $\mathcal{O}(\Delta x^2)$, as shown in [14] for the wave equation without damping and the choice of the BIOR2.2 wavelet basis with $\bar{m} = 2$ vanishing moments.

Tables 1 and 2 also show the high memory saving obtained with the proposed compression technique. For the wave equation without damping, we note the effectiveness of the compression when the BDF2 rule is used. In the case of the physical parameters of silicon, the standard compression technique $\mathcal{S}$ has a null memory saving.

Remark 5.1. In numerical experiments, we have observed similar errors and the same EOC and memory saving when we consider the Neumann problem (2.2) with datum $g(\mathbf{x};t) = t^4 e^{-t} \cos(x_1^2 + 2x_2^2)$.

Remark 5.2. It is known that a key issue of time-domain BEMs is the capability for retrieving accurate solutions when long times T are considered. To show how the compression strategy influences the accuracy of the approximation in such cases, we have applied the proposed scheme for the choice of the larger value $T = 40$. In the same setting of Table 1, we report the results obtained for the BIOR2.2 wavelets, the basis that displays the lower compression rate because of the lower number of vanishing moments. We have computed the reference solutions $\varphi_{M_e,N_e}(\mathbf{x};t)$ and $u_{M_e,N_e}(\mathbf{x};t)$ with $M_e = 256$ subintervals for the discretization of the parametrization interval $(-\pi, \pi]$ and $N_e = 8192$ subintervals for the time interval $[0, 40]$. In Table 3 we report the accuracy of the solution computed with the same choice of the discretization parameters of the reference one and for different choices of the threshold parameter ε. As expected, the corresponding errors increase as the compression increases. Moreover we point out that the memory savings are higher than those shown in Table 1, for both the choices of the CQ ODE solvers, since a higher number of time steps N has been considered. It is worth noting that, in accordance with what was observed in Remark 3.1, the TRAP solver allows for a lower compression and, if the larger parameter $\varepsilon = 1.0\text{E} - 08$ is chosen, too many entries of the BEM matrices are neglected with a consequent totally inaccurate solution. Similar comments are valid for the other choices of the wavelets basis.

TABLE 3

Wave equation without damping ($c = 1 \cdot {}^{m}/_{s}$ and $\alpha = 0 \cdot {}^{m^2}/_{s}$). Errors and memory saving for the wavelet BIOR2.2 compression and for different thresholds. $T = 40$.

	$\varepsilon = 1.0\text{E}-12$			$\varepsilon = 1.0\text{E}-10$			$\varepsilon = 1.0\text{E}-08$		
	$E_{\varphi}^{M_e,N_e}$	$E_{u}^{M_e,N_e}$	$\text{mem}_{\text{BIOR2.2}}^{\mathcal{W}}$	$E_{\varphi}^{M_e,N_e}$	$E_{u}^{M_e,N_e}$	$\text{mem}_{\text{BIOR2.2}}^{\mathcal{W}}$	$E_{\varphi}^{M_e,N_e}$	$E_{u}^{M_e,N_e}$	$\text{mem}_{\text{BIOR2.2}}^{\mathcal{W}}$
BDF2	$2.90\text{E}-05$	$6.84\text{E}-07$	92.8%	$5.06\text{E}-04$	$5.42\text{E}-06$	97.2%	$4.99\text{E}-02$	$6.52\text{E}-04$	98.8%
TRAPEZ	$1.24\text{E}-03$	$2.21\text{E}-07$	56.0%	$3.20\text{E}-02$	$3.18\text{E}-04$	82.2%	$1.74\text{E}+44$	$1.49\text{E}+30$	95.8%

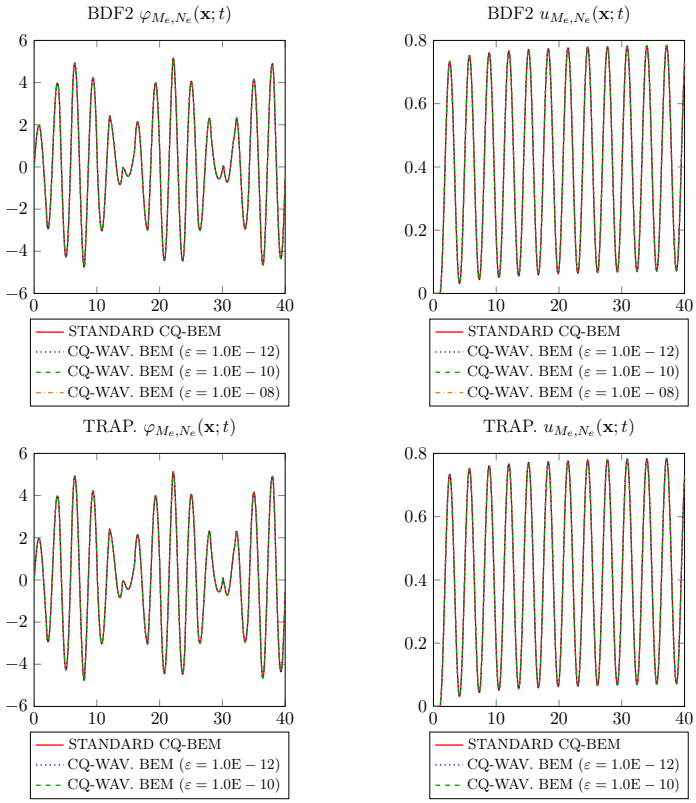

FIG. 9. *Wave equation without damping ($c = 1 \cdot {}^{m}/_{s}$ and $\alpha = 0 \cdot {}^{m^2}/_{s}$). Temporal profiles of φ_{M_e,N_e} (left plots) and u_{M_e,N_e} (right plots) for the standard and wavelet BIOR2.2 CQ-BEM. $T = 40$.*

Finally, we have not observed any increase or decrease in the effective damping with respect to the compression rate. As proof of this, we consider a nonvanishing oscillating wave, solution of (2.1) for the pure wave equation, with datum $f(\mathbf{x};t) = \sin(t)^2$, $t \in [0, 40]$, and all parameters of Table 3. We note that, with such a choice of the datum, the solution is constant with respect to the space variable. In Figure 9 we show the behavior of the density function $\varphi_{M_e,N_e}(\mathbf{x};t)$, $\mathbf{x} = (0,0)$, and of the potential $u_{M_e,N_e}(\mathbf{x};t)$, $\mathbf{x} = (2,0)$, with respect to the time variable. We compare the reference (standard) solution with those obtained by applying the wavelet BIOR2.2 CQ-BEM associated to the BDF2 and TRAP rules, by varying the parameter ε. As we can see, up to reasonable values ε (see Table 3), no spurious damping effects are visible.

5.2. Application to some realistic problems. In this section, we apply the approach presented in the previous sections to some numerical examples. In particular, in Examples 1 and 2 we solve two scattering problems: the former with a Dirichlet datum (soft scatterer) and the latter with a Neumann one (hard scatterer). Finally, in Example 3 we consider a Neumann problem, corresponding to the propagation of a wave generated by a load. We present the results for the choice of the BDF2 CQ-BEM approach and the BIOR6.8 wavelet matrix compression.

Example 1. We consider the scattering of an incident wave $u_{\text{inc}}(\mathbf{x};t)$ by an infinitely long cylindrical scatterer, immersed in a medium with wave propagation velocity $c = 1 \cdot {}^{\text{m}}/_{\text{s}}$ and damping parameter $\alpha = 10 \cdot {}^{\text{m}^2}/_{\text{s}}$ (which, after a proper scaling, correspond to the parameters of brass; see [42]). In a fixed 3D Cartesian coordinates system (x_1, x_2, x_3), the cylindrical scatter is supposed to be sound-soft and invariant with respect to x_3 and to have a kite-shaped section. We consider a cylindrical incident wave due to a causal signal $\lambda(t) = 10000 \cdot \sin(4t) \cdot e^{-1.6(t-3)^2}$, simultaneously emitted by all the points in a line source parallel to the x_3-axis. Therefore, the incident wave is invariant to x_3 and the problem is reduced to a 2D case. Consequently, we choose to set our simulation in the plane $x_3 = 0$, where the boundary of the section of the scatterer is $\Gamma := \{\mathbf{x} = (x_1, x_2) \in \mathbf{R}^2 \ : \ \mathbf{x} = (\cos\theta + 0.65(\cos 2\theta - 1), 1.5\sin\theta),\ \theta \in (-\pi, \pi]\}$. According to the above assumptions, the incident wave is obtained as time convolution of the forward fundamental solution (2.3) of the damped wave equation and the signal $\lambda(t)$, i.e.,

$$u_{\text{inc}}(\mathbf{x} : t) = \int_0^t G(\|\mathbf{x} - \mathbf{x}_{\text{S}}\|; t - \tau)\lambda(\tau)d\tau, \qquad \mathbf{x} \in \mathbf{R}^2 \setminus \{\mathbf{x}_{\text{S}}\},\ t \in [0, T]. \tag{5.5}$$

The source point on the line source is chosen as $\mathbf{x}_{\text{S}} = (1.24, 1.24)$ and $T = 15$ is the final observation time. The datum of the Dirichlet TD-BIE (2.5) is $g(\mathbf{x};t) = -u_{\text{inc}}(\mathbf{x};t)$. In the following, $u_{\text{inc}}(\mathbf{x};t)$ will be evaluated by using the Lubich CQ method. The time interval of interest is subdivided into $N = 2^{10}$ subintervals. For the space discretization, we choose to decompose the parametric interval $(-\pi, \pi]$ in $M = 2^{10}$ subintervals. We set the threshold parameter $\varepsilon = 1.0E - 08$, with a consequent memory saving of 99.89%. In Figure 10, we show the behavior of the density function on the boundary Γ of the kite-shaped section, i.e., we report $\varphi((\cos\theta + 0.65(\cos 2\theta - 1), 1.5\sin\theta); t)$ for $\theta \in (-\pi, \pi]$ and $t \in [0, 15]$. The left plot is its 2D view, while the right plot is its 3D view.

Finally, we use the single layer space-time integral potential representation (2.4) to reconstruct the scattered field $u_{\text{sca}}(\mathbf{x};t)$. In Figure 11 we plot the time history of

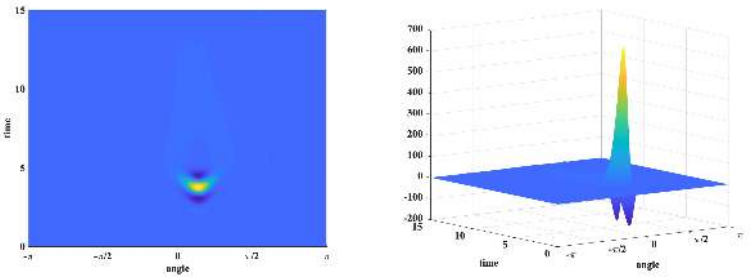

FIG. 10. *Example* 1. *2D (left plot) and 3D view (right plot) of* $\varphi((\cos\theta + 0.65(\cos 2\theta - 1), 1.5\sin\theta); t)$ *for* $\theta \in (-\pi, \pi]$ *and* $t \in [0, 15]$.

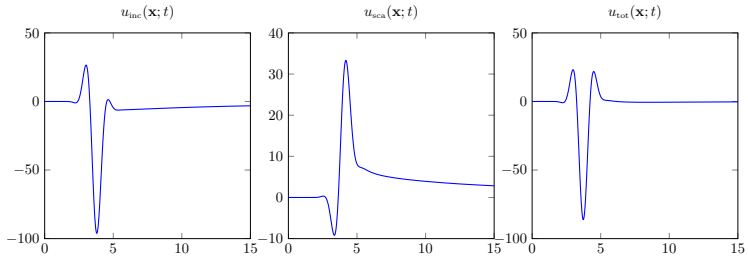

FIG. 11. *Example* 1. *Temporal profile of the incident field* $u_{inc}(\mathbf{x};t)$*, the scattered field* $u_{sca}(\mathbf{x};t)$*, and the scattered total* $u_{tot}(\mathbf{x};t)$ *at the point* $\mathbf{x} = (0.75, 0.75)$.

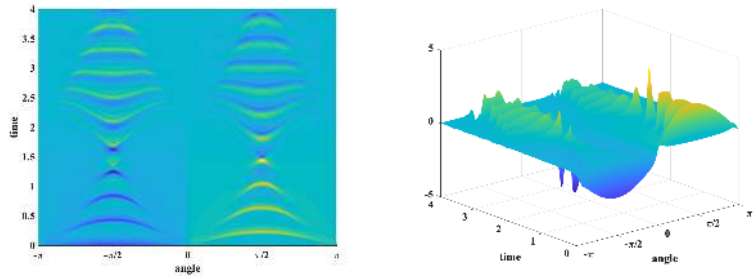

FIG. 12. *Example* 2. *2D (left plot) and 3D view (right plot) of* $\varphi((\cos\theta, 0.1\sin\theta);t)$ *for* $\theta \in (-\pi, \pi]$ *and* $t \in [0, 4]$.

the incident field $u_{\rm inc}(\mathbf{x};t)$ (left), of the scattered field $u_{\rm sca}(\mathbf{x};t)$ (center), and of the total field $u_{\rm tot}(\mathbf{x};t)$ (right), given by the sum of $u_{\rm inc}$ and $u_{\rm tot}$, at the exterior point $\mathbf{x} = (0.75, 0.75)$.

Example 2. We consider the hard-scattered field $u_{\rm sca}(\mathbf{x};t)$ of a plane vertically propagating incident wave $u_{\rm inc}(\mathbf{x};t)$, impinging upon an elliptical crack $\Gamma := \{\mathbf{x} \in \mathbf{R}^2 \ : \ \mathbf{x} = (\cos\theta, 0.1\sin\theta),\ \theta \in (-\pi, \pi]\}$. Here, we refer to a domain where the wave propagation velocity is $c = 1 \cdot {\rm m/s}$ and there is no damping, i.e., $\alpha = 0 \cdot {\rm m^2/s}$. The type of $u_{\rm inc}(\mathbf{x};t)$ is assumed as a Ricker wavelet

$$h(t) = A\left[2\pi^2 f_{\rm P}^2 t^2 - 1\right] e^{-\pi^2 f_{\rm P}^2 t^2},$$

where $f_{\rm P} = 1.5$ and $A = 0.6$. The incident wave $u_{\rm inc}(\mathbf{x};t) := h(x_2 - x_{0,2} + c(t - t_0))$ is centered at the point $\mathbf{x}_0 = (0, x_{0,2})$ with $x_{0,2} = -1 \cdot {\rm m}$, and it is emitted with a time shift parameter $t_0 = 1 \cdot {\rm s}$. We solve the Neumann TD-BIE (2.6) with the datum $g(\mathbf{x};t)$ on Γ consisting of the normal derivative of $u_{\rm inc}(\mathbf{x};t)$. We remark that this datum is similar to that considered in [3], where the problem is studied for different geometries of the crack. We choose a decomposition of the parametric interval $(-\pi, \pi]$ of the crack Γ into $M = 2^{10}$ subintervals and a discretization of the time interval of interest $[0, 4]$ into $N = 2^{10}$ subintervals. The threshold parameter is $\varepsilon = 1.0{\rm E}-08$, which gives rise to a memory saving of 97.46%. In Figure 12, we plot the behavior of the approximate density function on the boundary Γ of the crack, i.e., $\varphi((\cos\theta, 0.1\sin\theta);t)$, for $\theta \in (-\pi, \pi]$ and $t \in [0, 4]$.

To reconstruct the scattered field $u_{\rm sca}(\mathbf{x};t)$, we use (2.4). In Figure 13, we show the behavior in time of the incident field $u_{\rm inc}(\mathbf{x};t)$, the scattered field $u_{\rm sca}(\mathbf{x};t)$, and the total field $u_{\rm tot}(\mathbf{x};t)$ at the exterior point $\mathbf{x} = (0, 0.4)$. We recall that $u_{\rm tot}(\mathbf{x};t)$ is obtained by the superposition of $u_{\rm inc}(\mathbf{x};t)$ and $u_{\rm sca}(\mathbf{x};t)$.

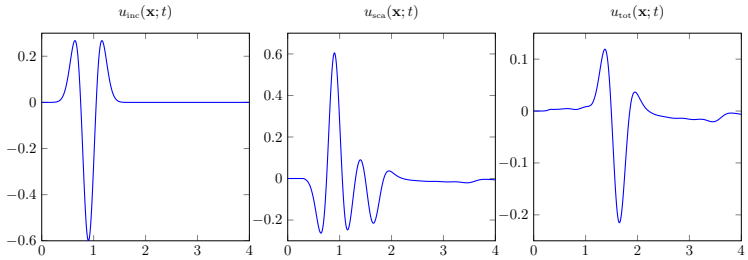

FIG. 13. *Example* 2. *Temporal profile of the incident field* $u_{inc}(\mathbf{x};t)$*, the scattered field* $u_{sca}(\mathbf{x};t)$*, and the scattered total* $u_{tot}(\mathbf{x};t)$ *at the point* $\mathbf{x} = (0, 0.4)$.

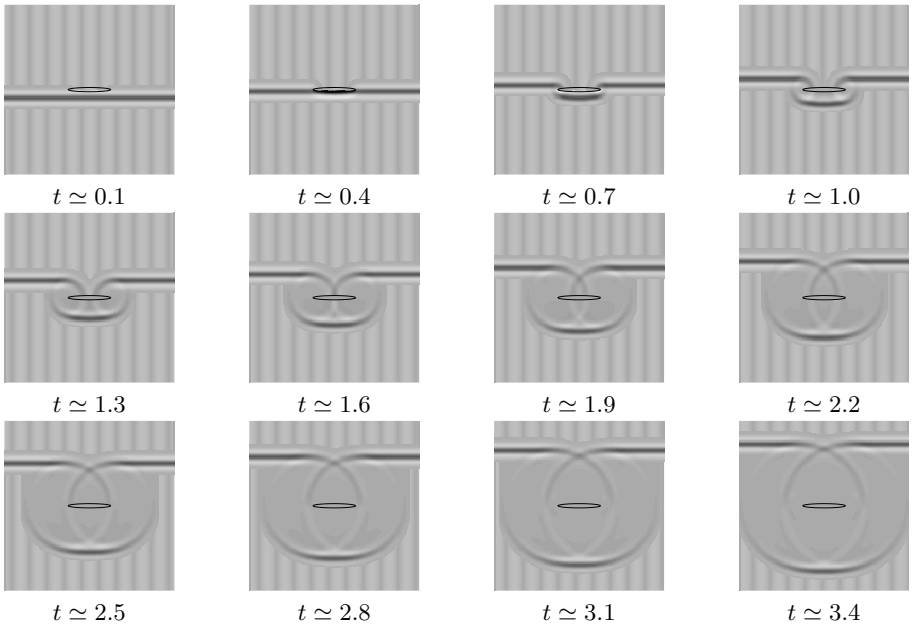

FIG. 14. *Example* 2. *Snapshots of the reconstructed total field* $u_{tot}(\mathbf{x};t)$ *around the elliptic crack.*

Finally, several snapshots related to the reconstructed total field in a square around the crack for different time instants are presented in Figure 14. These results show how the incident wave reaches the crack and how the total field is affected by the scattered wave. In particular, we observe a diffraction caused at the edges of the ellipse, whose effects are visible on both the upper and the lower half of the square. At the beginning of the simulation, the total field vanishes on the upper part of the ellipse, due to the interaction of the incident and the scattered waves. Then, as time passes, the scattered wave diminishes and the wavefront recovers, even if the effects of the diffraction are still present as a shadow. Our results are in perfect agreement with those presented in [3].

Example 3. We consider an infinite thin plate with an elliptic hole $\Gamma := \{\mathbf{x} \in \mathbf{R}^2 \ : \ \mathbf{x} = (\cos\theta, 0.1\sin\theta),\ \theta \in (-\pi, \pi]\}$, whose center is set at the origin of a fixed Cartesian coordinates system. We simulate a wave generated by two loads, located at the points $\mathbf{x}_1 = (\sqrt{2}/2, \sqrt{2}/20)$ and $\mathbf{x}_2 = (-\sqrt{2}/2, \sqrt{2}/20)$ on Γ, and decaying exponentially in time, i.e., we consider the Neumann TD-BIE (2.6) with datum

$$g(\mathbf{x};t) = 10\,[\delta(\mathbf{x}-\mathbf{x}_1)+\delta(\mathbf{x}-\mathbf{x}_2)]\,e^{-t^2}, \tag{5.6}$$

where $\delta(\mathbf{x})$ stands for the Dirac delta distribution. The velocity is $c = 632\cdot\,\mathrm{m/s}$, which refers to the second sound velocity for nonporous glass [42]. With this choice of the data, we consider two examples: a wave propagation problem without (case a) and with (case b) the damping. The chosen threshold parameter is $\varepsilon = 1.0\mathrm{E}-08$. For the spatial discretization we subdivide the parametric interval $(-\pi,\pi]$ of Γ into $M = 2^{10}$ subintervals and for the time discretization we fix $N = 2^{10}$ equispaced time instants within the interval $[0,4]$.

Case a. As the first case, we suppose that there is no damping, i.e., $\alpha = 0\cdot\,\mathrm{m^2/s}$. In Figure 15, we show the behavior of the approximate density function on the boundary Γ of the crack, i.e., $\varphi((\cos\theta, 0.1\sin\theta);t)$, for $\theta\in(-\pi,\pi]$ and $t\in[0,4]$. By using the single layer space-time integral potential representation (2.4), we compute the approximate solution $u(\mathbf{x};t)$ at the points $\mathbf{x}=(0,1)$, $\mathbf{x}=(0,2)$, and $\mathbf{x}=(0,-1)$. The corresponding time histories are plotted in Figure 16. We remark that $u(\mathbf{x};t)$ has the same behavior at all three points and there is no transient phase before the wave reaches these observation points. In spite of the high number of spatial discretization points, we observe a memory saving of 99.99% compared to the standard CQ-BEM. In Figure 17 we show some snapshots of the solution $u(\mathbf{x};t)$ at different time instants of the interval $[0,1]$ and in the x_1x_2-domain $[-4,4]\times[-4,4]$, external to the hole. We observe that the two loads generate two waves that act separately at the beginning of the simulation. Then, as time increases, their interaction contributes to the pick of $u(\mathbf{x};t)$, until the solution starts to decay exponentially in time as the Neumann datum does.

Case b. In the second example, we assume $\bar\tau = 10^{-12}\cdot\,\mathrm{s}$ such that $\alpha = 2.5\times10^6\cdot\,\mathrm{m^2/s}$, as in [42]. The time behavior of $u(\mathbf{x};t)$ at the points $\mathbf{x}=(0,1)$, $\mathbf{x}=(0,2)$, and

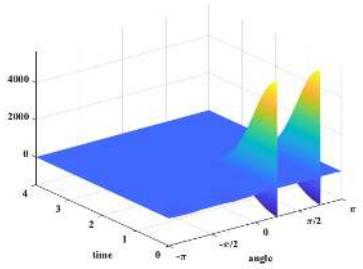

FIG. 15. *Example* 3. *Case* a. *3D view of* $\varphi((\cos\theta,0.1\sin\theta);t)$ *for* $\theta\in(-\pi,\pi]$ *and* $t\in[0,4]$.

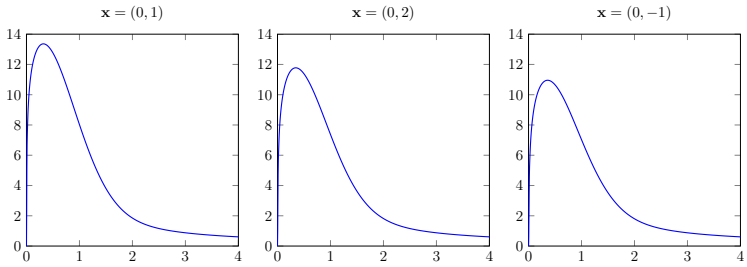

FIG. 16. *Example* 3. *Case* a. *Temporal profile of* $u(\mathbf{x};t)$ *at the points* $\mathbf{x}=(0,1)$ *(left),* $\mathbf{x}=(0,2)$ *(center), and* $\mathbf{x}=(0,-1)$ *(right).*

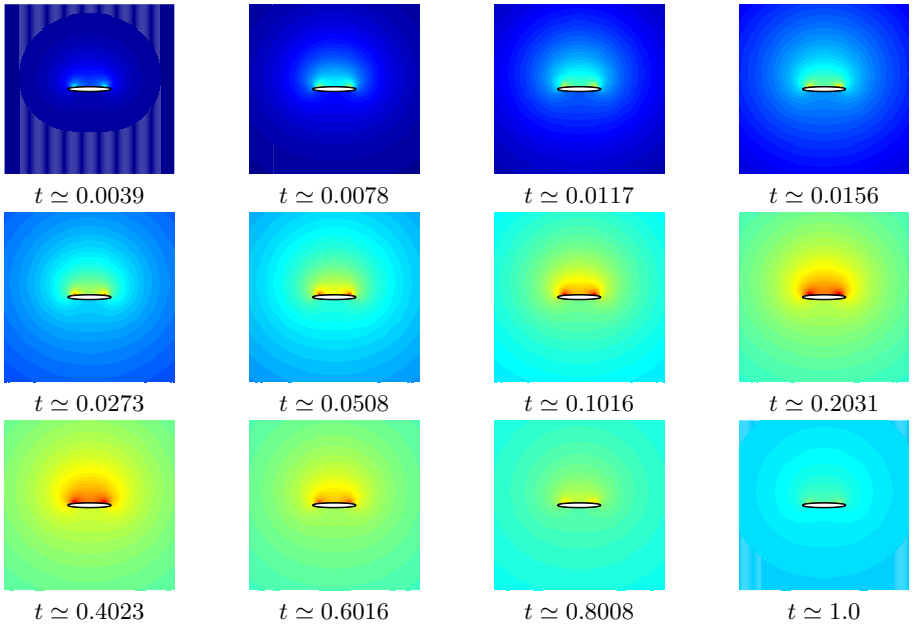

FIG. 17. *Example* 3. *Case* a. *Snapshots of* $u(\mathbf{x};t)$ *around the hole.*

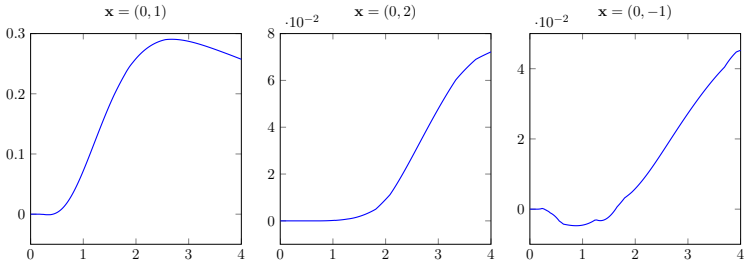

FIG. 18. *Example* 3. *Case* b. *Temporal profile of* $u(\mathbf{x};t)$ *at the points* $\mathbf{x} = (0,1)$ *(left),* $\mathbf{x} = (0,2)$ *(center), and* $\mathbf{x} = (0,-1)$ *(right).*

$\mathbf{x} = (0,-1)$, represented in Figure 18, shows a transient phase (which is absent when $\alpha = 0 \cdot \mathrm{m}^2/\mathrm{s}$) of the wave before the observation points are reached.
We remark that the global memory saving in this case is 99.94%. From the snapshots in Figure 19, we see that there is a long transient phase during which the generated waves do not interact and the effects of the two loads are located in the upper half square. In the lower part, the total wave is confined very close to the boundary of the hole, due to the dissipation.

6. Conclusions and perspectives. We have considered two boundary integral reformulations of the wave equation with damping in 2D unbounded domains for Dirichlet and Neumann type boundary conditions. For the resolution of the corresponding BIEs, we have used a Galerkin method in space coupled with second order Lubich convolution quadratures in time, and we have applied a wavelet compression technique to sparsify the matrices of the resulting global discretization. Based on the fast DWT for the accurate and efficient computation of the integrals involving wavelet

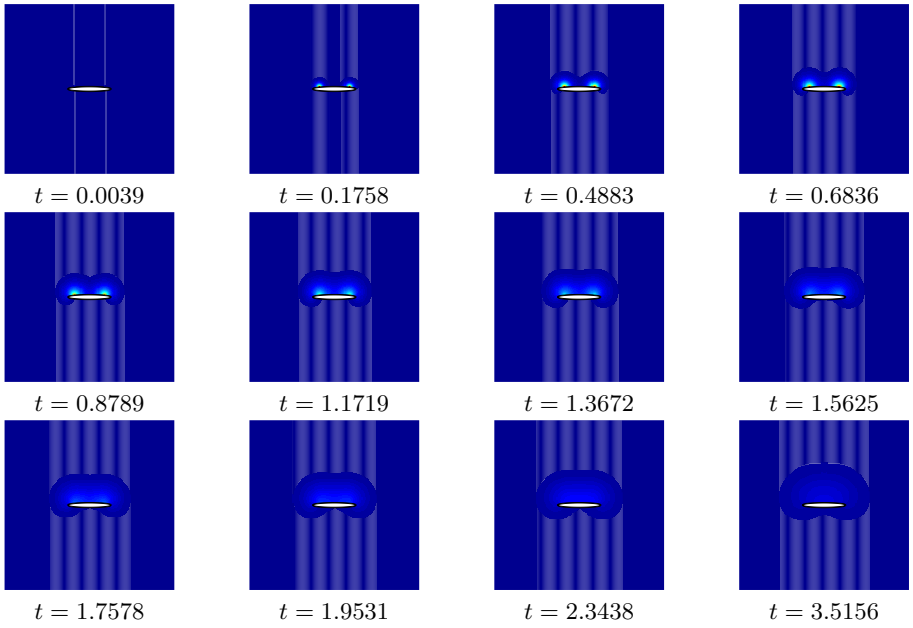

FIG. 19. *Example* 3. *Case* b. *Snapshots of* $u(\mathbf{x};t)$ *around the hole.*

functions, we have proposed a numerical procedure that allows for a compression of the wavelet BEM matrices without the need for storing a priori the fully populated ones. The proposed approach allows us to use wavelet bases of any type, with a high number of vanishing moments, that do not need to be known in closed form, and to consider CQ based on any stable ODE solver. From extensive numerical testing, we have considered, as benchmark wavelet bases, the biorthogonal BIOR2.2 and BIOR6.8 and the Daubechies DB10 and DB45 functions and, as benchmark ODE solvers, the trapezoidal rule and the BDF of order 2. The numerical testing we have performed shows the effectiveness of the wavelet compression of the matrices associated to the single and double layer operators for all choices of the wavelet basis. With respect to the discretization parameters, such a compression results in growth less than linear when the damping parameter is small compared to the speed of wave propagation (for example, for silicon) or in linear growth when the damping parameter is big compared to the speed of wave propagation. The numerical results we have obtained show an optimal L^2 global convergence rate, even when a very high sparsification of the matrices is retrieved.

We believe that the proposed approach displays potential also for what concerns the application of BEM wavelet methods to 3D wave propagation problems, where the sparsification of the matrices is even more crucial. Indeed, wavelet compression techniques can be generalized to the 3D case by using wavelet basis functions defined on surfaces. Successful results have been obtained, for example, in [36], where stationary problems are considered. For what concerns 3D time dependent problems, it is worth mentioning that the sparsification property of the BEM matrices has been analyzed for the pure wave equation and with the use of the standard piecewise linear local basis functions; we refer the reader, for example, to [32], [7], [28]. In these papers suitable assumptions on the data of the problem or on the geometry of the obstacle and on the transient phase are considered. Moreover, as for the 2D case, the

mentioned methods rely on the analytic expression of the CQ coefficients associated to particular ODE solvers. We believe that an investigation in this direction is worthy and that a pure numerical black box approach, as the one proposed here in two dimensions, could be considered to solve 3D time dependent problems as well.

Acknowledgment. The authors are grateful to the referees for their careful reading of the manuscript and their useful comments.

REFERENCES

[1] T. Abboud, P. Joly, J. Rodríguez, and I. Terrasse, *Coupling discontinuous Galerkin methods and retarded potentials for transient wave propagation on unbounded domains*, J. Comput. Phys., 230 (2011), pp. 5877–5907.

[2] A. Aimi and M. Diligenti, *A new space-time energetic formulation for wave propagation analysis in layered media by BEMs*, Internat. J. Numer. Methods Engrg., 75 (2008), pp. 1102–1132.

[3] A. Aimi, M. Diligenti, and S. Panizzi, *Energetic Galerkin BEM for wave propagation Neumann exterior problems*, CMES Comput. Model. Eng. Sci., 58 (2010), pp. 185–219.

[4] A. Aimi, M. Diligenti, and C. Guardasoni, *Energetic BEM for the numerical analysis of 2D Dirichlet damped wave propagation exterior problems*, Commun. Appl. Ind. Math., 8 (2017), pp. 103–127.

[5] A. Aimi, M. Diligenti, and C. Guardasoni, *Energetic BEM for the Numerical Solution of 2D Hard Scattering Problems of Damped Waves by Open Arcs*, Springer INdAM Ser., 30, Springer, New York, 2019, pp. 267–283.

[6] A. Bamberger and T. Ha Doung, *Formulation variationelle espace-temps pour le calcul par potentiel retardé da la difraction d'une onde acoustique*, Math. Methods Appl. Sci., 8 (1986), pp. 405–435.

[7] L. Banjai and S. Sauter, *Rapid solution of the wave equation in unbounded domains*, SIAM J. Numer. Anal., 47 (2008), pp. 227–249.

[8] L. Banjai, *Multistep and multistage convolution quadrature for the wave equation: Algorithms and experiments*, SIAM J. Sci. Comput., 32 (2010), pp. 2964–2994.

[9] L. Banjai and M. Schanz, *Wave propagation problems treated with convolution quadrature and BEM*, in Fast Boundary Element Methods in Engineering and Industrial Applications, Lect. Notes Appl. Comput. Mech. 63, Springer, New York, 2012, pp. 145–184.

[10] L. Banjai and V. Gruhne, *Efficient long-time computations of time-domain boundary integrals for 2D and dissipative wave equation*, J. Comput. Appl. Math., 235 (2011), pp. 4207–4220.

[11] L. Banjai and M. Kachanovska, *Fast convolution quadrature for the wave equation in three dimensions*, J. Comput. Phys., 279 (2014), pp. 103–126.

[12] L. Banjai and M. Kachanovska, *Sparsity of Runge-Kutta convolution weights for the three-dimensional wave equation*, BIT, 54 (2014), pp. 901–936.

[13] L. Banjai, M. López-Fernández, and A. Schädle, *Fast and oblivious algorithms for dissipative and two-dimensional wave equations*, SIAM J. Numer. Anal., 55 (2017), pp. 621–639.

[14] S. Bertoluzza, S. Falletta, and L. Scuderi, *Wavelets and convolution quadrature for the efficient solution of a 2D space-time BIE for the wave equation*, Appl. Math. Comput., 366 (2020), 124726, doi:10.1016/j.amc.2019.124726.

[15] G. Beylkin, R. Coifman, and V. Rokhlin, *Fast wavelet transforms and numerical algorithms.* I, Comm. Pure Appl. Math., 44 (1991), pp. 141–183.

[16] S. Chaillat, L. Desiderio, and P. Ciarlet, Jr., *Theory and implementation of $\mathcal{H}$-matrix based iterative and direct solvers for oscillatory kernels*, J. Comput. Phys., 351 (2017), pp. 165–186.

[17] A. Cohen, I. Daubechies, and J. Feauveau, *Biorthogonal bases of compactly supported wavelets*, Comm. Pure Appl. Math., 45 (1992), pp. 485–560.

[18] I. Daubechies, *Ten Lectures on Wavelets*, CBMS-NSF Regional Conf. Ser. in Appl. Math. 61, SIAM, Philadelphia, 2004.

[19] L. Desiderio, *An $\mathcal{H}$-matrix based direct solver for the boundary element method in 3D elastodynamics*, in AIP Conference Proceedings, 1978, 120005.

[20] K. Eppler and H. Harbrecht, *Fast wavelet BEM for 3D electromagnetic shaping*, Appl. Numer. Math., 54 (2005), pp. 537–554.

[21] S. Falletta, G. Monegato, and L. Scuderi, *A space-time BIE method for nonhomogeneous exterior wave equation problems. The Dirichlet case*, IMA J. Numer. Anal., 32 (2012), pp. 202–226.

[22] S. Falletta, G. Monegato, and L. Scuderi, *A space-time BIE method for wave equation problems: The (two-dimensional) Neumann case*, IMA J. Numer. Anal., 34 (2014), pp. 390–434.
[23] S. Falletta and G. Monegato, *An exact non reflecting boundary condition for 2D time-dependent wave equation problems*, Wave Motion, 51 (2014), pp. 168–192.
[24] S. Falletta and G. Monegato, *Exact non-reflecting boundary condition for 3D time-dependent multiple scattering-multiple source problems*, Wave Motion, 58 (2015), pp. 281–302.
[25] S. Falletta and L. Scuderi, *A new boundary element integration strategy for retarded potential boundary integral equations*, Appl. Numer. Math., 94, (2015), pp. 106–126.
[26] S. Falletta and S. Sauter, *The panel-clustering method for the wave equation in two spatial dimensions*, J. Comput. Phys., 305 (2016), pp. 217–243.
[27] S. Falletta, *BEM coupling with the FEM fictitious domain approach for the solution of the exterior Poisson problem and of wave scattering by rotating rigid bodies*, IMA J. Numer. Anal., 38 (2018), pp. 779–809.
[28] S. Falletta, G. Monegato, and L. Scuderi, *On the discretization and application of two space-time boundary integral equations for 3D wave propagation problems in unbounded domains*, Appl. Numer. Math., 124 (2018), pp. 22–43.
[29] L. Greengard and V. Rokhlin, *A new version of the fast multipole method for the Laplace equation in three dimensions*, Acta Numer., 6 (1997), pp. 229–269.
[30] W. Hackbusch, *The panel clustering technique for the boundary element method*, in Mathematical and Computational Aspects. Boundary Elements IX9, C. A. Brebbia, W. L. Wendland, and G. Kuhn, eds., Springer, New York, 1987, pp. 463–474.
[31] W. Hackbusch and Z.P. Nowak, *On the fast matrix multiplication in the boundary element method by panel clustering*, Numer. Math., 54 (1989), pp. 463–491.
[32] W. Hackbusch, W. Kress, and S. Sauter, *Sparse convolution quadrature for time domain boundary integral formulations of the wave equation*, IMA J. Numer. Anal., 29 (2009), pp. 158–179.
[33] H. Harbrecht and R. Schneider, *Wavelet Galerkin schemes for 2D-BEM*, in Problems and Methods in Mathematical Physics, Oper. Theory Adv. Appl. 121, Birkhäuser, Basel, 2001, pp. 221–260.
[34] H. Harbrecht and R. Schneider, *Biorthogonal wavelet bases for the boundary element method*, Math. Nachr., 269-270 (2004), pp. 167–188.
[35] H. Harbrecht and R. Schneider, *Wavelet Galerkin schemes for boundary integral equations: Implementation and quadrature*, SIAM J. Sci. Comput., 27 (2006), pp. 1347–1370.
[36] H. Harbrecht and M. Randrianarivony, *Wavelet BEM on molecular surfaces: Solvent excluded surfaces*, Computing, 92 (2011), pp. 335–364.
[37] G. C. Hsiao and A. Rathsfeld, *Wavelet collocation methods for a first kind boundary integral equation in acoustic scattering*, Adv. Comput. Math., 17 (2002), pp. 281–308.
[38] W. Kress and S. Sauter, *Numerical treatment of retarded boundary integral equations by sparse panel clustering*, IMA J. Numer. Anal., 28 (2008), pp. 162–185.
[39] C. Lage and C. Schwab, *Wavelet Galerkin algorithms for boundary integral equations*, SIAM J. Sci. Comput., 20 (1999), pp. 2195–2222.
[40] Y. Liu, A.C. Yücel, H. Bağci, A.C. Gilbert, and E. Michielssen, *A wavelet-enhanced PWTD-accelerated time-domain integral equation solver for analysis of transient scattering from electrically large conducting objects*, IEEE Trans. Antennas Propagation, 66 (2018), pp. 2458–2470.
[41] Ch. Lubich, *On the multistep time discretization of linear initial-boundary value problems and their boundary integral equations*, Numer. Math., 67 (1994), pp. 365–389.
[42] E. Marin, L.S. Vaca-Oyola, and O. Delgado-Vasallo, *On thermal waves' velocity: Some open questions in thermal waves' physics*, Rev. Mex. Fis. E, 62 (2016), pp. 1–4.
[43] G. Monegato, L. Scuderi, and M.P. Stanic, *Lubich convolution quadratures and their application to problems described by space-time BIEs*, Numer. Algorithms, 56 (2011), pp. 405–436.
[44] G. Monegato and L. Scuderi, *A space-time BIE method for 2D mixed wave equation problems*, Appl. Math. Comput., 259 (2015), pp. 1046–1070.
[45] M. Schanz, *Fast multipole method for poroelastodynamics*, Eng. Anal. Bound. Elem., 89 (2018), pp. 50–59.